Senescence-Related Changes to the Lipid Composition of SH-SY5Y Cells with Implications for α-Synuclein Misfolding

By Elise Førsund

Thesis submitted in partial fulfilment of the requirements for the degree of Master of Science

Department of Biological Sciences
Faculty of Mathematics and Natural Sciences
University of Bergen

June 2020

Acknowledgments

This project was carried out in the NucReg research program at the Department of Biological Sciences, University of Bergen, in the time period August 2019 – May 2020.

First, I would like to thank my supervisor Øyvind Halskau for introducing me to this very interesting topic and for always taking the time (preferably over coffee) to thoroughly answer all of my questions. Your sincere interest for science is evident and undoubtedly inspirational! I also want to add that answering my emails, even at midnight, is not something I take for granted.

Next, I want to thank my co-supervisor Espen Bariås for teaching me all there is to know about cell culturing, and for always coming up with new solutions when things have not gone as planned. I greatly value all of the time you have spent teaching me all the necessary techniques at the lab, answering all my questions and for repeatedly (!) showing me were all the lab-equipment/solutions are. Although not my co-supervisor on paper, I would also like to thank Martin Jakubec for assisting with the NMR and MS part of the thesis, as well as continuing to answer my emails, even after your time here at the University had ended. I hope that someday I will understand NMR and MS half as good as you do. A special thank should also be given to Thomas Stevenson and Sushma Grellscheid for providing the senescence methodology and helping us implement it. It would not have been a very interesting assignment without your input!

This whole journey has been a blast, much owed to the great work environment at NucReg, my fellow students (/friends) and the coffee machine at the lunchroom. Lastly, a shout out to friends and family for the continuously moral support and for showing interest, despite having some problems comprehending and pronouncing the word “molecular biology”.

Bergen, June 2020

Elise Førsund

Table of Contents

Selected Abbreviations

AA – arachidonic acid

AD - Alzheimer's disease

DA – dopaminergic

DHA – docosahexaenoic acid

FA – fatty acid

LC-MS/MS - liquid chromatography with tandem mass spectrometry

MUFA – monounsaturated fatty acid

NMR - Nuclear magnetic resonance

PA – glycerophosphates

PC – phosphatidylcholine

PD - Parkinson's disease

PE – phosphatidylethanolamine

PG – phosphatidylglycerol

PI – phosphatidylinositol

PUFA – polyunsaturated fatty acid

PS – phosphatidylserine

SA-β-gal - senescence-associated β-galactosidase activity

SFA – saturated fatty acid

SM – sphingomyelin

SN - substantia nigra

SCD - stearoyl-CoA-desaturase

α-Syn – α-Synuclein

ABSTRACT

Along with an increasing life expectancy in the population comes more incidences of age-associated disorders like Parkinson's disease (PD), affecting 1% of the population over the age of 60 to as high as 5% over the age of 85. At the molecular level, PD is characterized by the gradual loss of dopaminergic neurons and the presence of protein aggregates in the affected surviving cells. These aggregates consist of misfolded α-Synuclein (α-Syn), a protein located in presynaptic terminals of neurons, existing in an equilibrium between soluble and membrane-bound form. It is proposed that the membrane-bound form of the protein also modulates its aggregation propensity, making the lipid membrane an interesting focus of PD research. As aging is the most well-established risk factor for developing the disease, this thesis aimed to search for age-related changes to the lipid composition of neurons, which could help explain why old cells are more prone to α-Syn misfolding and aggregation.

To mimic the molecular characteristics of the aging cell, cellular senescence was induced in the neuroblastoma SH-SY5Y cell line using the cytotoxic anticancer agent etoposide. Lipid profiling was achieved using a combination of solution-phase ^{31}P NMR and LC-MS/MS. As a result, interesting findings were made, including a 37% and 19% senescence-related increase in the abundance of phosphatidylinositol (PI) and phosphatidylserine (PS), which are negatively charged lipids implicated in α-Syn binding. Additionally, LC-MS/MS detected a senescence-related decrease of 10.4% in the overall polyunsaturated fatty acid (PUFA) content, in particular the polyunsaturated omega-6 fatty acid arachidonic acid (AA, 20:4), a fatty acid involved in the growth and repair mechanisms of neurons. Other interesting findings regarding the fatty acid composition were a 14.0% decrease in the stearic/oleic acid (18:0/18:1) ratio, as some researchers now claim that oleic acid may worsen α-Syn pathology. Some slight changes were also observed in the overall length of the fatty acids, of which short acids of 10-12 carbons were observed in the senescence-induced cells and not in the untreated cells, a result which also could be of relevance for PD as misfolding of α-Syn has reported to only occur in the presence of short hydrocarbon chains. Overall, our findings were in line with existing knowledge regarding age-induced lipid changes. Although few of these findings were significant or alone can explain why aging poses the greatest risk factor for developing PD, they do suggest that aging changes the lipid environment in neurons, possibly to one that is more susceptible for the neuronal toxicity mechanisms associated with PD.

1. INTRODUCTION

Neurodegenerative disorders are among the most prevalent and least understood conditions of our time, making them an important target of research. Neurodegeneration is the progressive loss of neuron integrity, potentially leading to death of the cell. As most neurons do not reproduce or replace themselves, their loss can cause irreversible physical or cognitive disability in a manner dependent on the population of neurons affected. In many neurodegenerative diseases, a mutual pathological hallmark is the accumulation of misfolded proteins [1]. Upon misfolding, the exposure of buried hydrophobic regions within these proteins can drive their aggregation - creating oligomeric molecular entities that are toxic to the cell[2]. Having a limited capacity to clear out misfolded proteins, neurons are particularly vulnerable to these toxic accumulations, explaining why most of these protein misfolding diseases occur in the brain[3]. Some of the most common neurodegenerative disorders associated with protein misfolding are Alzheimer's disease (AD) and Parkinson's disease (PD), both mainly occurring in the elderly. Although there is a growing body of research regarding the aggregation mechanism of these proteins, the correlation between the aging cell and the misfolding process is still poorly understood. This knowledge could be crucial in the understanding of the fundamental molecular origin of these diseases and contribute in the quest to search for a cure.

1.1 Parkinson's Disease

PD is the second most common neurodegenerative disorder after AD, and it is estimated that 7-10 million people worldwide suffers from this disease to which there is no cure or efficient methods for early diagnosis[4,5]. Typical symptoms associated with PD include shaking, stiffness and problems with movement. Additionally, a variety of non-motor symptoms can be observed as early as 12-14 years before the patient experiences any of the typical PD symptoms. This period is referred to as the prodromal phase and symptoms include obesity, sleep disturbance, constipation, depression and fatigue[6]. Although most prevalent amongst the elderly, some people are diagnosed before the age of 50, in which the disease is referred to as early-onset PD. According to the American Parkinson Disease Association, early-onset PD accounts for 10-20 % of all diagnosed with the disease, and about half of those are diagnosed before the age of 40.

1.1.1 Risk Factors for Developing PD

Even though the exact cause of PD is still unknown, scientists have discovered several factors increasing a person's risk of developing the disease including age, gender, race, diet, environmental factors, head traumas and genetic factors[7-10]. Among these, age poses the greatest risk factor by far (Figure 1.1.1). Table 1.1.1 presents an overview and explanations of the most common risk factors associated with PD.

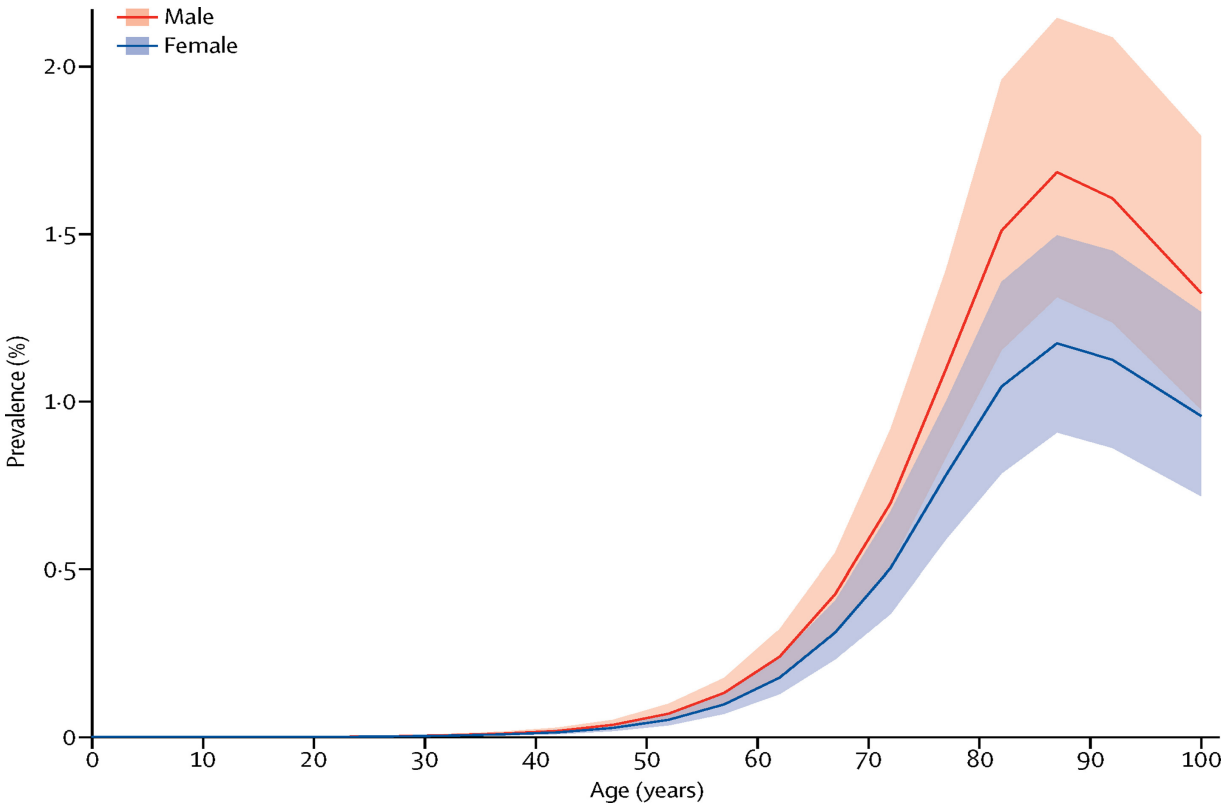

Figure 1.1.1. Global prevalence of Parkinson's disease in 2016. Prevalence of the disease is represented as the percentage of the global population affected. Most people with the disease are between 85-90 years old, and the greater proportion of the affected are men (orange). Shading indicates 95% uncertainty intervals. The figure is retrieved from an article in Lancet Neurol 2018, by Parkinson's Disease Collaborators[11].

Table 1.1.1 – Description of risk factors associated with PD

Risk factors	Prevalence
Age	Prevalence of PD increases from 1% of the population over the age of 60, to as high as 5% over the age of 85[10], making getting older the greatest risk factor for developing PD, by far.

Gender	There is significant differences in the prevalence of PD by sex, being 3.2 times more prevalent in men than in woman[12]. Theories to explain these differences include (i) a protective effect of estrogen in woman, (ii) differences in lifestyle (higher rate of head trauma and more frequent exposure to occupational toxins in men) or (iii) genes on the sex chromosomes[13].
Race	PD is twice as common in Whites compared to Blacks and Asians, with Hispanics having the highest incidences of PD world wide[14]. These findings argue for differences in genetic susceptibility to PD.
Diet	A growing body of evidence suggests that calorie restrictions have a definite neuroprotective effect[15]. Polyunsaturated fatty acids (PUFAs), coffee and tea have also been linked to neuroprotection, whilst dairy products have been suggested to have the opposite effect[7].
Environmental factors	Urban areas have higher prevalence of PD, suggesting a relationship between the exposure to various environmental factors and the development of the disease[14]. Indeed, several studies have found associations between the exposure to pesticides and PD incidences[16,17].
Head traumas	Although research results have been somewhat inconsistent, a number of studies have shown a link between PD and trauma to the head and neck. In a twin study, of whom only one had PD, the disease more often appeared in the twin who had previously suffered a head injury[8]. Even more interesting, the association was stronger in monozygotic than in dizygotic twins.
Genetic factors	Several genetic mutations have been associated with PD, including mutations in the *LRRK2*, *GBA* and *SNCA* genes[18]. The

	resulting mutants alter signal transmission (*LRRK2*), disturb the degradation of proteins – leading to protein accumulation (*GBA*) and causes elevated levels and/or altered function of α-Syn (*SNCA*). At least 30 associated mutations have been identified within the *SNCA* gene alone, emphasizing the role of α-Syn in PD[18].

1.1.2 Neuropathological Hallmarks of PD: α-Synuclein Aggregates and Dopaminergic Neuronal Loss

At the molecular level, hallmarks of PD include the gradual loss of dopaminergic (DA) neurons in the substantia nigra (SN) and the presence of protein aggregates termed "Lewy bodies" in the affected surviving cells[10]. The SN is a part of the brain important for controlling movement and reward, and the loss of its DA neurons leads to the motor-dysfunctional symptoms associated with PD. There is also a great amount research suggesting that the disease may affect the lower brainstem structures before spreading to the SN, explaining the non-motor symptoms in the prodromal phase of PD[6].

Lewy bodies mainly consist of a small, intrinsically disordered protein called α-Syn[19,20]. In neurons, α-Syn is predominantly found in presynaptic terminals and is thought to be involved in neurotransmitter release through interactions with the lipid membrane [21]. Although its exact biological role is still somewhat unclear, α-Syn seems to regulate vesicle packaging and trafficking[22]. Structurally, α-Syn consists of three distinct regions including (i) an amphipathic N-terminal region, (ii) a central hydrophobic region, as well as (iii) a highly acid C-terminal tail[23]. Among these, the central hydrophobic region, called the non-amyloid-β component (NAC) region, seems to be involved in protein aggregation[24].

Under normal physiological conditions, monomeric α-Syn exists in equilibrium between water-soluble and membrane-associated form, both functional[25]. This folding propensity is due to the proteins intrinsically disordered nature, meaning it does not have a distinct tertiary structure and can adopt numerous conformations depending on its environment. However, this structural characteristic also allows these proteins to easily interact with other monomers

of themselves, potentially leading to oligomerization and subsequently fibril formation (Figure 1.1.2).

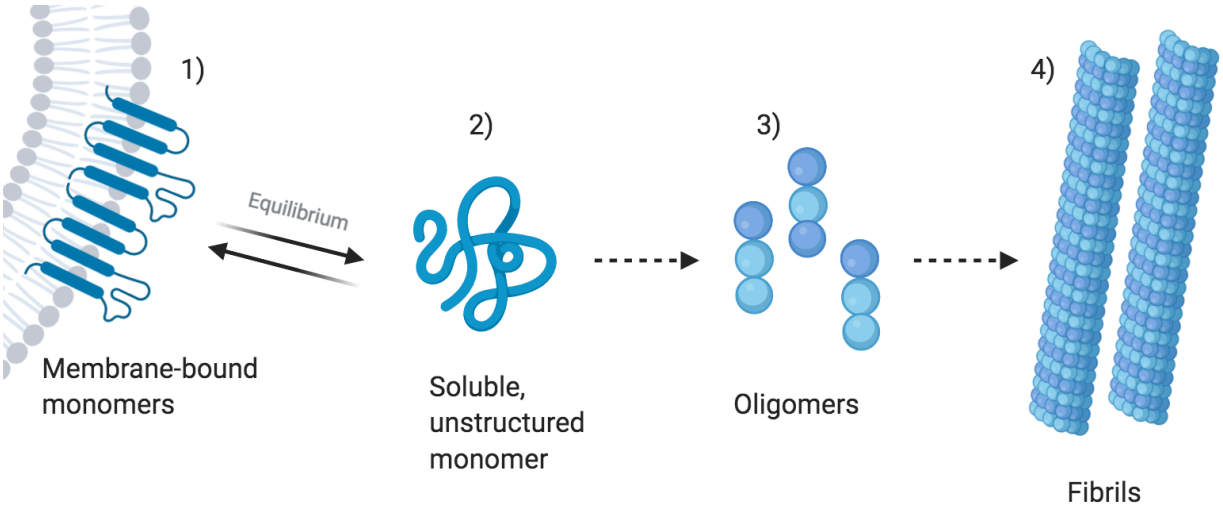

Figure 1.1.2 - α-Syn fibril-formation. At normal conditions, monomeric α-Syn exists in an equilibrium between water-soluble and membrane-associated (1) and water-soluble form (2). Upon pathogenesis, misfolded monomers interact with each other, creating toxic oligomers (3) and subsequently fibrils (4). The illustration is created in BioRender.com.

Regarding their degenerative effect, several toxicity mechanisms have been proposed - many of which concerning interactions with the lipid membrane. *In vitro* cell experiments have demonstrated that α-Syn oligomers can create pores in the lipid bilayer thereby increasing permeability and causing a depolarization of the cell membrane, presumably due to an influx of ions from the exterior of the cell[26]. While the native monomeric protein normally exists in the presynaptic terminals of neurons, fibrils and their oligomeric intermediates can be found throughout the cell body, possibly disrupting membranes of multiple organelles – in addition to the plasma membrane[26]. Although still debatable, oligomers seem to be more toxic than both α-Syn in monomeric and fibrillary form [27].

1.2 The Role of the Lipid Membrane in Protein Misfolding Diseases

Accounting for half of the brain's dry weight, lipids are an important area of research when investigating brain-related issues. In the body, these molecules have multiple functions including storing energy, acting as messengers in signaling and being structural components of cell membranes[28]. As there is virtually no energy storage in the brain, most brain lipids

have signaling and structural roles, being components of the bilayer surrounding cells and organelles.

Due to the wide span of functions performed by the human brain, cells of the nervous system show great functional and structural diversity. This diversity is partly achieved by the unique lipid profiles of the individual populations of neurons[28,29]. In membranes, lipid composition affects curvature, charge and fluidity - enabling a diversity of membrane structures with varying functions. However, this differing lipid composition of neuronal membranes could also explain why some neurons are more vulnerable to degeneration than others. More specifically, why the SN is the brain region affected by α-Syn aggregates, and why the most affected region in AD is the CA1 region of the hippocampus[30]. Unfortunately, studies trying to find a link between these particular brain regions and protein misfolding propensity, generally do not look at the lipid membrane even though it may be involved in two central parts of the disease by (i) catalyzing the misfolding process and (ii) being a target for the toxic effects of the aggregates[26,31].

1.2.1 Brain Lipid Composition

Membrane lipids is a collective term for all lipids involved in forming the double-layered surface of all cells, termed the lipid bilayer. There are three major classes of membrane lipids including phospholipids, glycolipids and cholesterol[32]. Among these, phospholipids are the most abundant components and consist of one or two long hydrocarbon chains (hydrophobic) linked to a phosphorylated head group (hydrophilic), resulting in an amphiphilic characteristic necessary for forming the lipid bilayer. These head groups consist of either glycerol or sphingosine, giving rise to phosphoglycerides and sphingomyelin (SM), respectively. Examples of phosphoglycerides are phosphatidic acid (PA), phosphatidylcholine (PC), phosphatidylethanolamine (PE), phosphatidylserine (PS), phosphatidylglycerol (PG), cardiolipin (CL) and phosphatidylinositol (PI). Quantitatively, the most abundant phospholipids in the brain are PE (~35-36%), followed by PC (~30%) and PS (~17%)[33].

Concerning their hydrocarbon chains, phospholipids of cell membranes have a high content of polyunsaturated fatty acids (PUFAs)[32]. Neuronal cell membranes are particularly enriched in long PUFAs, mainly docosahexaenoic acid (DHA, 22:6) and arachidonic acid (AA, 20:4). Although primarily esterified to phospholipids, these fatty acids (FAs) can be released from

the membrane and function as highly active signaling molecules. As PUFAs are derived from diet, changes in dietary intake can alter brain levels and thus the signaling pathways they regulate[34].

1.2.2 α-Synuclein-Membrane Interaction

In regard to PD, lipids are becoming increasingly relevant as accumulating amount of studies now emerge on the relationship between the lipid membrane and the aggregation process of α-Syn. As mentioned in section 1.1.2, α-Syn normally exists in an equilibrium between water-soluble and membrane-associated form (Figure 1.1.2) and although the latter appears to contribute to the protein's functional role, membrane binding has also been shown to modulate its aggregation propensity[35]. Soluble and disordered α-Syn binds to the membrane by interacting with lipid head groups – causing a conformational change in the protein with some regions forming α-helical structures (Figure 1.2.2)[36,37]. This conformational change happens due to the presence of five potential amphipathic α-helices identified in the N-terminal region of α-Syn[38]. Four of these five helices are structurally similar to lipid-binding motifs found in apolipoproteins - the proteins that bind lipids to form lipoproteins, transporting lipids in the blood, cerebrospinal fluid and lymph. These helixes allow binding to a variety of lipid assemblies including lipid vesicles, membranes and micelles[35]. As the N-terminal of α-Syn is a positively charged region, the protein prefers membranes with a highly negatively charged lipid content[39,40]. Other membranes that have an increased likelihood of α-Syn binding include those with lipid packing defects and membranes in fluid phase[41,42].

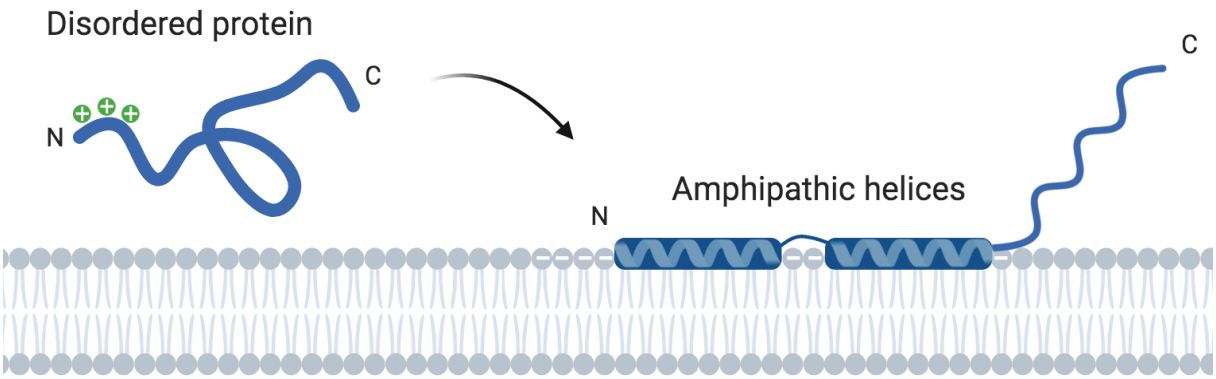

Figure 1.2.2 – The membrane-binding process of α-Syn. The positively charged N-region of natively unfolded α-Syn interacts with negatively charged lipids of the membrane, adapting an amphipathic helical structure. The illustration is created in BioRender and is inspired by a figure by Mori *et al*t [38].

1.2.3 Parameters Affecting Aggregation Propensity

While the binding mechanism of α-Syn to the membrane is well described, it is still not fully understood how this binding can modulate the aggregation process of the protein. Three parameters seem to be the main contributors to this propensity: the chemical properties of the lipids, their physical state and the protein/lipid ratio[25].

Although evidence shows that α-Syn preferably binds to negatively charged lipids and membranes in fluid phase, it is uncertain whether or not these factors affect the aggregation propensity or just the binding affinity[38,3]. In fact, some studies have actually found that a more fluid membrane prevents α-Syn from aggregating, suggesting a positive correlation between membrane fluidity and protein homeostasis[43]. Nevertheless, a greater correlation has been drawn between the length of the lipid's FA chains and the protein aggregation tendency. Indeed, when using model systems composed of various anionic lipids, membrane-induced aggregation was only enhanced in the presence of lipids with short FA chains[41]. Although these chemical properties definitely are of high pathological relevance, more recent experiments suggest that the lipid/protein ratio may be of even more importance[44,45].

In environments with high protein concentrations compared to lipids, the presence of negatively charged lipids seem to induce aggregation[25] (Figure 1.2.3). This may be due to an insufficient amount of available binding places on the lipid membrane, leaving α-Syn monomers to compete for binding, resulting in a local up-concentration of the protein. Already bound α-Syn could then serve as a nucleation site by using these extra monomers to promote oligomerization. Also, it is believed that the lack of distance between these bound α-Syn can bring their exposed NAC-regions in close proximity, further accelerating the fibril nucleation process[42]. At opposite ratios, on the other hand, no fibril formation is observed seeing as all soluble monomers have been adsorbed at the membrane surface[25]. In regards to early-onset PD, this is interesting seeing as many of these cases are caused by α-Syn gene duplication – possibly increasing the protein/lipid ratio[36].

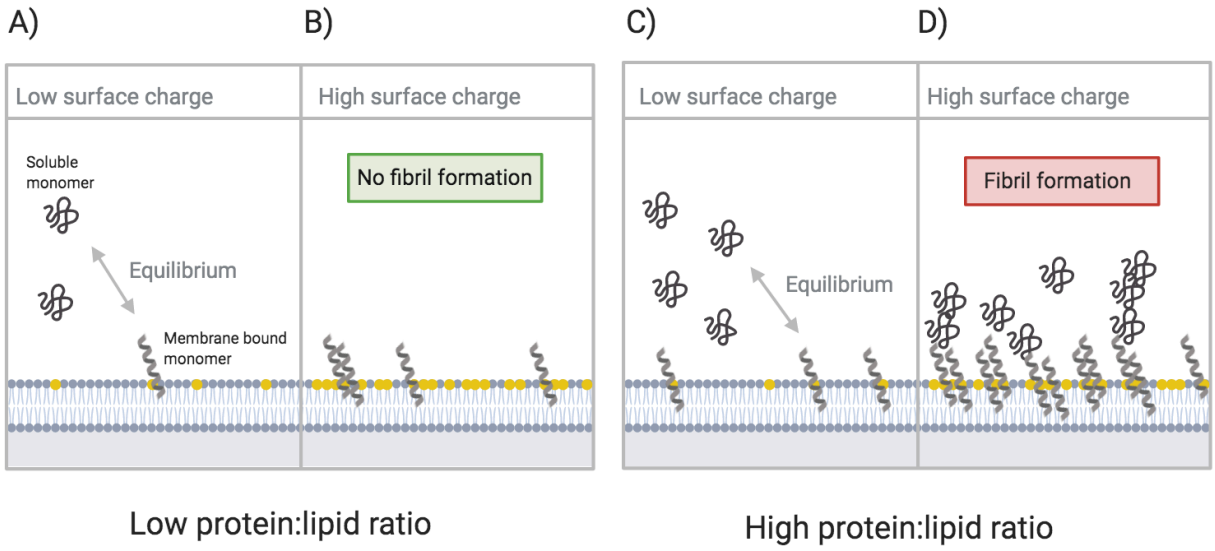

Figure 1.2.3 - Parameters affecting α-Syn membrane binding and aggregation propensity. Four scenarios are depicted showing the probability of fibril formation with regard to membrane surface charge and accessibility. In membranes of low negatively charged lipid content (panel A and C), an equilibrium between soluble and membrane bound α-Syn monomers occurs, which seems to have limited effect on nucleation and fibril formation. In a scenario with high surface charge combined with a low protein/lipid ratio, most monomers are absorbed to the membrane surface, leaving no free monomers available for fibril formation (panel C). In contrast, in a combination of high protein/lipid ratio and surface charge (panel D), the lack of distance between the bound monomers can bring several monomers in close proximity, promoting the fibril nucleation process. The high protein/lipid ratio also means that free monomers are available for fibril elongation on the already bound monomers. The figure is made in BioRender.com and is inspired by a figure made by Viennet *et al*[42].

1.2.4 Implications for Synaptic Transmission

In addition to its barrier function, this bilayer enclosing cells serves many important roles including cellular signaling. Synaptic transmission is a common form of cellular signaling and occurs when a nerve impulse is transferred to an adjacent neuron by the release of neurotransmitters – like dopamine[46]. Vesicles loaded with these neurotransmitters fuse with the cell membrane and thereby release its content to the exterior of the cell. This process largely depends on synaptic proteins, making them a target of research in synaptic transmission. However, the importance of the lipid environment in which they operate, it is now becoming clearer. Lipid composition at synapses differs from the rest of the cell membrane, suggesting that synaptic proteins require specific habitats for optimal function[47]. In regards to PD this is interesting seeing as synaptic abnormalities occur long before the actual loss of cell bodies[22]. Changes in lipid membrane composition could possibly change synaptic structure and function thus altering signaling transmission, eventually leading to the decline in dopamine levels. Establishing factors responsible for these changes in lipid

composition could therefore provide great insight into understanding the pathogenic causes of protein misfolding diseases. Looking at the greatest risk factor of them all, aging may be an important phenomenon to consider.

1.3 The Aging Brain

Being the main risk factor for developing PD, it is important to study the pathological changes to the aging brain at a molecular level, including any changes to lipid composition. Although no single cause of biological aging has yet been identified, researchers have proposed several theories, mainly falling into two categories: programmed and damage related. In the DNA damage theory of aging, it is proposed that aging merely is a consequence of accumulating DNA damage over time[48]. In this context, "damage" is referred to as naturally occurring alterations to the genetic material, resulting in dysfunctional gene products, which in turn causes an accumulation of problems at the molecular, cellular and organism level. Proponents of programmed aging, on the other hand, propose that aging is more complex and involves a number of pre-programmed aging-factors, following a predetermined set of instructions, such as certain hormones like growth hormone (GH) and insulin-like growth factor I (IGH-1) which both decline with age[49,50]. Seeing as the brain regulates the production of these hormones, some popular theories of aging propose that the brain acts as the master clock of each life stage, regulated by hormonal changes[51]. However, between those that argue for one or the other mechanism, there is some agreement concerning the biological changes that correlate with aging.

In the brain, the process of aging is associated with several structural, chemical and functional changes. Structural changes include loss of neuronal circuits and brain plasticity, changes in cell morphology and an overall decrease in brain mass[52]. Regarding the chemical changes, there seems to be an age-related reduction in levels of various neurotransmitters including dopamine, serotonin and glutamate[53]. Seeing as neurons use these chemical messengers to communicate, a decline results in numerous functional impairments including problems with movement, memory and learning difficulties, insufficient mood regulation and sleep disturbance.

Part of why the brain experiences so many age-related impairments, is because the nervous system is mainly composed of non- or infrequently replicating cells. Neurons for instance, have permanently blocked their capacity to proliferate once they are differentiated[54], which means that dead neurons may not get replaced. This can result in permanent cell loss and, if not properly repaired, cell damage in the remaining cells. For instance, as aging diminishes the body's repair mechanisms, damaged proteins may not get degraded by the proteasome, leaving misfolded proteins to accumulate in the cells[55]. Indeed, similar to PD brains, the presence of Lewy bodies and the progressive DA neuronal loss can also be observed in the SN of normal aging brains[56]. This brain region shows more pathological changes with normal aging compared to other regions like the hippocampus and hypothalamus, suggesting neurons in this region are especially vulnerable for degradation[10]. As previously mentioned, this varying vulnerability could be correlated to the differing lipid composition of individual cell types found in the brain.

1.3.1 Age-related Changes in Lipid Composition

All cells experience changes with aging, and these changes are also reflected in their lipids. Brain analysis reveals that the total amount of lipids decreases with age, but that this decrease is not evenly distributed throughout the brain regions or among the lipid species[57]. In one study, two lipids especially stood out, with an almost two-fold decrease compared to other lipids, and these were ethanolamine plasmalogen (PPE) and sphingomyelin (SM)[58]. Lipids like PI, PE and PC reveal a more moderate decrease of just 10% between the age of 40 and 100[58,59].

Not only does the total amount of lipids change with age, but also the chemical properties of the molecules, which are largely dependent on their FAs. Many of these changes are caused by nonenzymatic molecular modifications like lipid peroxidation, which is the oxidative degradation of lipids. In this process, highly reactive free radicals attack lipids in the cell membrane by "stealing" their electrons, forming FA radicals that in turn react with other FAs, subsequently producing lipid peroxides[60]. As PUFAs contain multiple double bonds, these FAs are at most risk at losing their electrons. Concerning aging, free radicals accumulate in cells as we age, increasing the rate of molecular modifications like lipid peroxidation. Indeed, several studies regarding age-related changes in FA composition, have observed an overall

decrease in PUFA simultaneously with an increase in monounsaturated fatty acids (MUFA)[61,62].

Most of these lipidomic studies use samples from a limited number of deceased individuals in the age group 20-100 years. One main concern using cells from test subjects is the cellular variation among the population as a result of different lifestyles, especially diet, and some genetic factors that may affect the lipid composition. Another consideration is the condition of the cells at the time the sample is taken as decomposing processes start radar rapidly after a person is deceased. These processes have been shown to also affect the lipids[63]. For example, some lipids are hydrolyzed shortly after death by lipases, freeing the FAs from their backbone[64]. As degradation continues, lipids are reduced to a mixture of saturated and unsaturated FAs, making it hard to conduct a precise composition study. One possible solution to eliminate these natural variations is to create a model system *in vitro* mimicking the aging cell.

1.3.2 Correlations Between Cellular Senescence and Aging

One of the hallmarks of cellular aging is the accumulation of senescent cells in various tissues throughout the body. Cellular senescence is defined as irreversible cell cycle arrest, meaning the cell is permanently unable to divide[65,66]. Senescence occurs in response to damaging stimuli to prevent the replication of damaged DNA which can be harmful to the cell. These stimuli include telomere shortening, oncogenic signaling and various forms of DNA damage[65]. With aging, telomere shortening is the main cause of cellular senescence, referred to as "replicative senescence". The biomolecular basis behind this type of senescence is that the sequence at the end of chromosomes, called telomeres, gets shorter for each division causing the cell to have limited replication potential. After a certain number of divisions, critically short telomeres initiate a DNA damage response triggering senescence[66].

In addition to their lack of ability to divide, senescent cells are characterized by several other factors including metabolic and morphological changes, chromatin reorganization and altered gene expression[67]. For instance, genes encoding proteins involved in the regulation of the cell cycle are upregulated in order to initiate the cell cycle arrest. Among these proteins are the cyclin-dependent kinases p16 and p21, of which their upregulation can be used as biomarkers

of senescence[67]. Regarding cell morphology, these cells display an irregular, flattened and enlarged shape compared to normal dividing cells, presumably due to larger cell components[68]. Higher lysosome content has also been reported in senescent cells, resulting in an elevated content of β-galactosidase, a eukaryotic hydrolase localized in the lysosome. This enzyme has an acidic pH optimum of 4.0-4.5, close to the natural milieu of the lysosome[69]. However, the increased enzyme activity in senescent cells makes it possible to detect the enzyme at a suboptimal pH of 6, referred to as senescence-associated β-galactosidase activity (SA-β-gal)[69]. X-gal, an analog of lactose, can be used for the identification of senescent cells in cell cultures, as this compound can be hydrolyzed by the enzyme resulting in an insoluble and intensely blue product[70]. Other cell components affected by senescence are lipids as several studies have associated senescence with an accumulation of specific triacylglycerols (TAGs), containing unsaturated, long fatty acyl chains. Regarding alterations to lipids of the cell membrane, on the other hand, less information is available, although replicative senescence is thought to be accompanied by several membrane-related phenotypic changes[71].

The fact that neurons are non-dividing cells means that they do not enter a state of replicative senescence – at least not in the same manner as their dividing counterparts. Still, there seem to be many similarities at the cellular level between aging and the process of senescence, suggesting that replicative senescence can be used as a model system for aging. Additionally, studies have emerged and accumulated on the correlation between astrocyte senescence and neurodegenerative diseases[72]. Astrocytes are non-neuronal support cells of the central nervous system, responsible for providing support and protection for neurons. Astrocytes are also thought to be involved in the secretion and absorption of neurotransmitters[73]. When astrocytes enter a state of senescence, they secrete metabolites of a senescence-associated secretory phenotype which is proposed to affect neighboring cells, like neurons, driving them to adopt a similar phenotype[72].

1.4 Methods for Lipid Analysis

In order to analyze changes in the lipid content of cells, a number of considerations have to be taken into account. For instants, given the structural diversity in lipid classes, it is not possible to accommodate all classes with a one-method-fits-all approach to lipid extraction, separation and detection.

1.4.1 Solvent Extraction of Lipids

When it comes to approaches used to extract lipids from biological samples, these can be divided into mechanical and chemical methods. Examples of mechanical methods are microwave-assisted extraction, oil press and ultrasonic-assisted extraction, whereas chemical methods include supercritical fluid extraction and solvent extraction[74]. Regarding the latter, the choice of solvents is highly dependent on the polarity of the lipid molecule of interest. Phospholipids, the main components of lipid membranes, are lipids of intermediate polarity and are typically extracted using a combination of organic solvents and water. This biphasic system allows water-soluble components like proteins and carbohydrates to be separated from the lipids, which remain in the organic phase.

The most commonly used solvent extraction methods are undoubtedly the Folch method and the Blight & Dyer method[75,76]. Both approaches are based on a biphasic separation system consisting of chloroform/methanol/water at varying ratios amongst the two methods. Chloroform and water make up the two phases, whilst methanol is added to improve the solubilization of membrane lipids by disrupting hydrogen bonding and electrostatic interactions between protein-lipids and lipid-lipids. After the lipid fraction has been collected, the solvents are removed using vapor, nitrogen gas or a combination of the two.

1.4.2 Nuclear Magnetic Resonance

An emerging powerful analytical tool for lipidomic studies is Nuclear Magnetic Resonance spectroscopy (NMR). The NMR principle is based on observing the behavior of excited nuclei after they are subjected to radiofrequency radiation[77]. This technique can only be used to study atomic nuclei with an odd number of protons and/or neutrons, giving them intrinsic nuclear magnetic movement and the possession of nuclear spins[78]. Moreover, the isotopes need to be naturally abundant or experimentally enriched in the molecules studied. In both hydrogen and phosphorus, the most abundant naturally occurring isotopes are magnetically susceptible. These isotopes are ^{1}H and ^{31}P and are both frequently used in NMR studies.

NMR as a method offers a very large array of techniques that have found use in practically all molecular disciplines, including analytical chemistry, metabolomics and lipidomics. One strength of NMR is the ability to uniquely resolve nuclei, even in complex samples. Under

certain conditions, it can also be used for absolute concentration determination of a given compound. Another advantage of NMR is that its non-destructive, allowing several analyses to be carried out on the same sample[77]. Nevertheless, one main disadvantage of NMR is its relatively low sensitivity, reflected in all the adaptations required to explore several lipid classes as well as the large amount of sample required for conducting the analysis. For this reason, NMR is primarily used to quantify the ^{31}Phosphorus-containing phospholipids. ^{31}P is a medium sensitivity nucleus that yields sharp lines and has a wide chemical shift range. When analyzing a ^{31}P NMR spectrum, moieties are matched with expected chemical shifts, expressed in parts-per-million (ppm). These chemical shift ranges of phosphorus are dependent on their chemical environment.

1.4.3 Mass Spectrometry

Another technique commonly used to analyze lipids is mass spectrometry (MS). MS can determine the mass of a molecule by measuring the mass-to-charge ratio (m/z) of its ions[77]. The results are presented in a mass spectrum – a plot of intensity as a function of m/z. Unlike NMR, the sensitivity of MS is high and detection limits reach nanomolar whilst only requiring a small amount of sample. Another advantage of MS is that it can be used for both selective (targeted) and nonselective (nontargeted) analysis, whereas NMR is generally used for nontarget analysis – like determining the overall composition of the sample. However, the method does have its limitations including more demanding sample preparation, lower resolution and no sample recovery.

In tandem mass spectrometry (MS/MS), an additional reaction step is performed to increase the ability to resolve and analyze the signals of complex samples. MS/MS combines two mass analyzers in one mass spec instrument. The first spectrometer (MS1) separates precursor ions according to their m/z ratio. Ions of particular m/z-ratios are then selected and split into smaller fragments before being introduced into MS2, which in turn separate and detect these fragments[79]. As each lipid has a unique fragmentation pattern, this additional fragmentation step allows for the separation and identification of compounds of very similar m/z-ratios (from MS1). Nevertheless, when the target molecule exists in a very complex mixture, MS alone may not be sufficient to perform the separation as several compounds may have similar molar mass and fragmentation patterns. This can be resolved by combining MS with another

separation process, such as liquid chromatography (LC). In LC-MS/MS, the sample is first injected into the LC-column where the different components of the solution travel at different speeds due to differing affinities for the stationary (coating on the inside of the column) and the mobile phase (the solvent passing through) of the column[79]. The resulting effluent is then ionized and directed into the MS/MS for detection. Seeing as MS can perform its actions in order of seconds, this detection can happen while LC is performing the initial chemical separation[80]. However, as many phospholipids will elute at almost the same time, many ions of different m/z-ratios will be ionized at the same time, but only a few can be selected for fragmentation in a single injection. As a consequence, some less abundant lipid species may be masked by lipids of higher concentrations at the same retention time (the time used for the lipid to pass through the chromatography column). One solution is the "iterative exclusion" (IE) strategy, which involves repeating the analysis on the same sample, excluding the previously selected ions[81].

LC-MS/MS data outputs include total ion chromatograms (sum of MS1 intensities over time), full MS1 spectra at different retention times and MS2 fragmentation spectra. To help interpret these data, scripts are often utilized. Scripts are basically just text files containing a set of commands and comments to help simplify the identification process. For instance, as each lipid species has a particular m/z value (based on the structure of the molecule) as well as a unique predicted fragmentation pattern, all of this information can be included to the script to help identify lipids of this origin.

2. AIMS

In order to get a better understanding of why age poses the greatest risk factor for developing several neurodegenerative disorders, including PD, one has to look for age-related alterations to the human brain at a cellular and molecular level. For this thesis, the target of research was age-related changes to the lipid composition of neurons. To form the aim several assumptions were taken into consideration:

1. There is a connection between the phospholipid composition of neurons and the misfolding process of α-Syn
2. Membrane lipid composition changes with age
3. Cellular senescence can be used as a model system for aging

Taking these assumptions into account, this thesis hypothesizes that the lipid composition of neuronal cells changes during aging and that these changes may contribute to the misfolding process of α-Syn.

3. MATERIALS

3.1 Instruments and Equipment

Table 3.1.1 - Instruments and equipment

Name	Application	Manufacturer
Allegra X-15R	Centrifugation	Beckman Coulter
BioSpin NEO600 Spectrometer	NMR	Bruker
Culturing dishes	Cell cultivation	Sarstedt
Dionex Ultimate 3000 UPLC	LC-MS/MS	Thermo Fisher
Eclipse Ts2 Inverted Microscope	Cell visualization	Nikon
Heraeus Pico 21	Centrifugation	Thermo Scientific
Micro Star 17R	Centrifugation	VWR™
Rotavapor R-100	Solvent evaporation	Buchi
TC10™ Cell Counter	Automatic cell counting	Bio-Rad
Thermo Q-Exactive Mass Spectrometer	LC-MS/MS	Thermo Fisher
TMS-F Microscope	Cell visualization	Nikon
Alpha 1-2 LD plus	Freeze drying	Christ

3.2 Reagents and Chemicals

Table 3.2.1 – All chemicals and reagents used

Name	Chemical formula	Supplier	Cat. #
Ammonium acetate	$NH_4CH_3CO_2$	Merck	1116
Acetonitrile	CH_3CN	Merck	00029
Citric Acid	$C_6H_8O_7$	-	-
Dichloromethane	CH_2Cl_2	Thermo Fisher Scientific	113460025
Dimethylformamide (DMF)	$(CH_3)NC(O)H$	-	-
Dimethyl sulfoxide (DMSO)	$(CH_3)_2SO$	Sigma-Aldrich	D8418

Disodium phosphate	Na_2HPO^4	-	-
Dulbecco´s Modified Eagle´s Medium	-	Sigma-Aldrich	F7524
Ethylenediaminetetraacetic acid (EDTA)	$C_{10}H_{16}N_2O_8$	Sigma-Aldrich	EDS
Etoposide	$C_{29}H_{32}O_{13}$	Sigma-Aldrich	E1383
Fetal bovine serum (FBS)	-	Sigma-Aldrich	F7524
Guanidinium chloride	CH_6ClN_3	-	-
Hydrochloric acid	HCl	-	-
Isopropanol	C_3H_8O	Sigma-Aldrich	34863
Magnesium Chloride	$MgCl_2$	Merck	05833
Methanol	CH_3OH	Merck	06035
Nitrogen gas	N	Praxair	500743
Penicillin streptomycin (PS)	-	Sigma-Aldrich	P0781
Potassium chloride	KCl	Sigma-Aldrich	P9541
Potassium hypophosphite	KH_2PO_2	-	-
Potassium ferrocyanide	$K_4[Fe(CN)_6]$	-	-
Sodium chloride (NaCl)	NaCl	VWR	27810
Sodium deoxycholate (DOC)	$C_{24}H_{40}O_4$	Sigma-Aldrich	D6750
Sodium hydroxide	NaOH	Merck	06498
Sodium dodecyl sulfate (SDS)	CH_3 $(CH2)$ $_{11}SO_4Na$	-	-
Thiourea	$SC(NH_2)_2$	-	-
Triethylammonium ions (TEAC)	$C_6H_{16}N^+$	-	-
Trimethylamine	C_3H_9N	-	-
Trypsin	-	Sigma-Aldrich	T2601
Polysorbate 20 **(**Tween-20)	$C_{58}H_{114}O_{26}$	-	-
X-Gal	$C_{14}H_{15}BrClNO_6$	-	-

3.3 Buffers and solutions

Table 3.3.1 - Prepared buffers and solutions

Dulbecco's Modified Eagle Medium (DMEM)	**CUBO solvent**
• 4500 mg/l Glucose, Sodiumpyruvate and Sodiumbicarbonat • 10 % FBS • 3 % L-glutamine • 1 % Penicillin Streptomycin (Pen Strep)	• 800 μM Guanidine chloride dissolved in DMF and TEA • 75% Dimethylformamide (DMF) • 25% Trimethylamine (TEA)

Guanidinium Chloride Thiourea (GCTU)	**4% Paraformaldehyde (PFA)**
• 6 M Guanidinium • 1.5 M Thiourea	• 1 M Sodium hydroxide • 10x PBS • 1 M Hydrochloric acid

10x Phosphate-buffered Saline (PBS)	**1x Dulbecco's PBS (D-PBS)**
• 80 g/l Sodium chloride • 2 g/l Potassium chloride • 20 g/l Sodium phosphate dibasic dihydrate • 4 g/l Potassium hypophosphite- pH 7.4	• 1x PBS • 0.1 g/l Calcium chloride • 0.1 g/l Magnesium Chloride

RIPA Buffer	**Sen-B-Gal Staining Solution**
• 150 mM Sodium chloride • 5 mM EDTA, pH 8.0 • 1% (v/v) NP-40 • 0.5% (w/v) Sodium deoxycholate (DOC) • 0.1% (w/v) Sodiumdodecyl sulfate (SDS) • 50 mM Tris, pH 8.0	• 1 mg/ml X-Gal • 40 mM Citric Acid/Sodium Phosphate- pH 6.0 • 5 mM Potassium Ferrocyanide • 150 mM Sodium Chloride • 2 mM Magnesium Chloride

Buffer A (LC-MS/MS)	**Buffer B (LC-MS/MS)**
• 40% acetonitrile • 60% water • 10 mM ammonium acetate	• 10% acetonitrile • 90% isopropanol • 10 mM ammonium acetate

3.4 Cell lines

Table 3.4.1 – The human cell lines used in the experiments

Cell line	Species	Tissue	Cell type	Supplier
SH-SY5Y	Human	Neuronal	Neuroblast	DSMZ: ACC-209
A-431	Human	Epidermis/skin	Epithelial	ATTC:CRL-1555

3.5 Software

Table 3.5.1 - Computer software and online resources used for result processing and analysis

Name	Use
Bruker TopSpin™ 4.0.7	NMR data processing and analysis
BioRender.com	Illustrations
LipMat script (Martin Jakubec *et al.*)	LC-MS/MS data processing
ImageJ	Cell image processing

4. METHODS

The main goal of this thesis was to study age-related changes to the lipid composition of neurons using a combination of ^{31}P NMR and LC-MS/MS, in hope of finding a correlation between aging, phospholipids and neurodegenerative disorders like PD. Figure 4.1 presents a schematic outline of the workflow in this thesis.

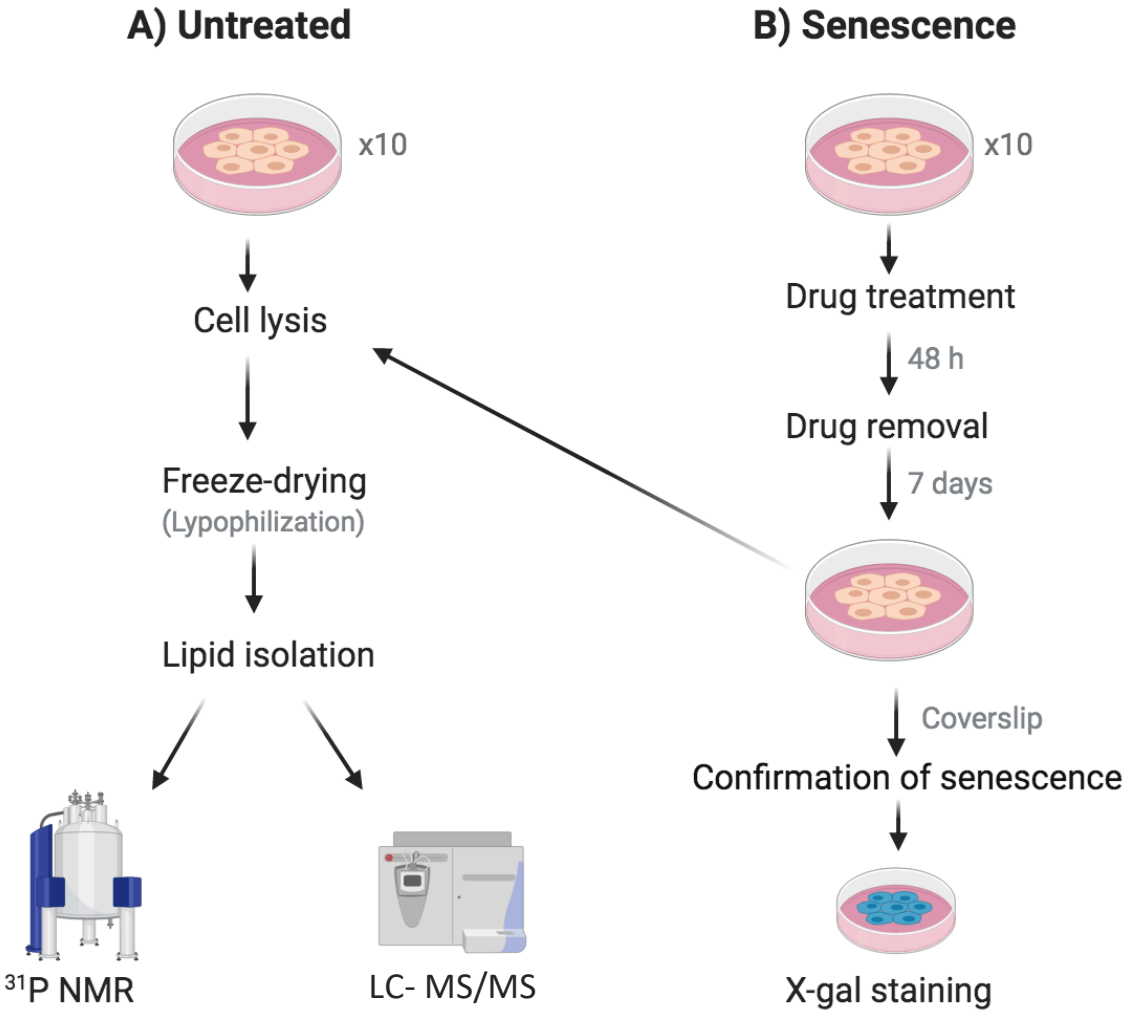

Figure 4.1 - Schematic overview of the main methodical steps in this thesis. A) Neuroblastoma SH-SY5Y cells were cultured, lysed and freeze-dried before the lipid fraction was extracted using a biphasic solvent system. ^{31}P NMR and LC-MS/MS was then performed for lipid profiling. B) For the induction of senescence, SH-SY5Y cells were incubated for 48h in etoposide followed by additional 7 days of incubation in fresh medium, in order to develop a senescent phenotype. X-gal staining was performed on coverslips to confirm the presence of senescent cells in the treated sample. The same procedure as in A) was then conducted on the senescent cells. The illustration is made in BioRender.com.

4.1 Cell Culture

The human-derived SH-SY5Y neuroblastoma cell line was chosen for this study, which is a cell line commonly used in PD research due to its intact neuronal properties, dopaminergic characteristics and ease of maintenance[82]. SH-SY5Y is a trice-subcloned cell line derived from the SK-N-SH cell line established from metastatic cells found in the bone marrow of a four-year-old girl in 1970[82]. Cultures of the SH-SY5Y cell line contain two distinct cell types: epithelial-like (flattened shape) and neuronal-like (stretched shape) (Figure 4.1.1). Furthermore, the cultures include both adherent and floating cells – both viable[83].

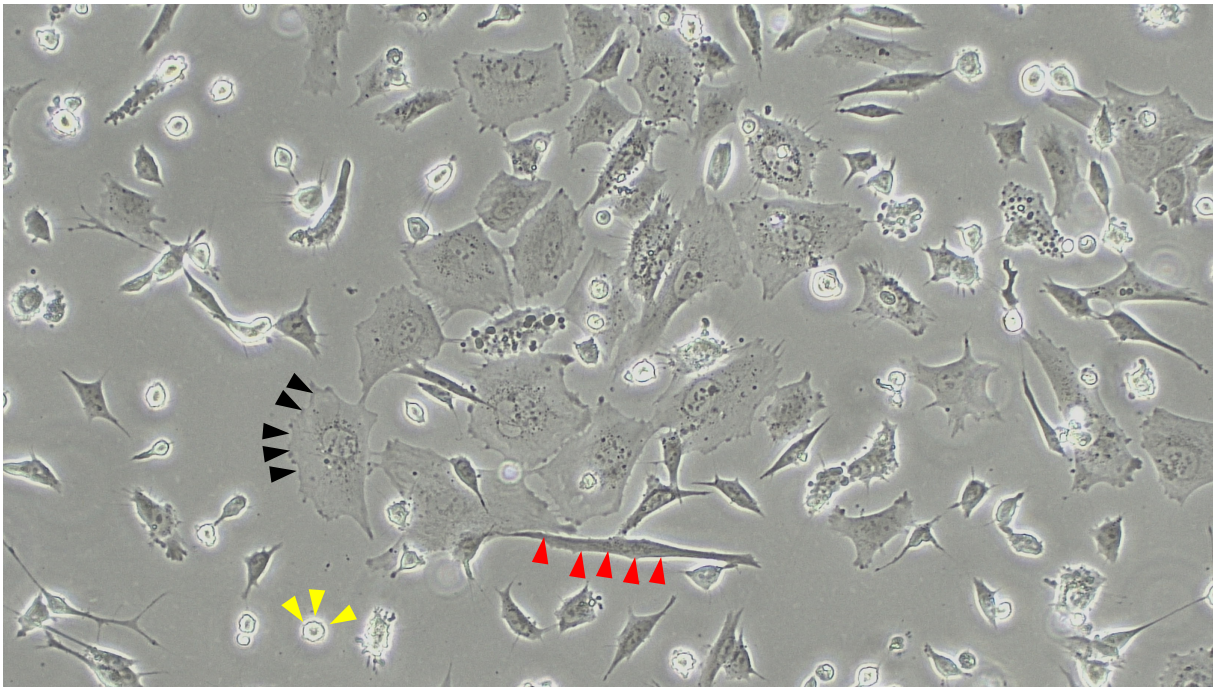

Figure 4.1.1 - Morphology of undifferentiated SH-SY5Y cells. The human neuroblastoma SH-SY5Y cells were cultured in Dulbecco's Modified Eagle's Medium (DMEM, Sigma), supplemented with 10% (v/v) fetal bovine serum (FBS, Sigma) and 1% (v/v) PenStrep (PS, Sigma). The culture contains epithelial-like (black arrowheads) and neuronal-like cells (red arrowheads), as well as both adherent and floating cells (yellow arrowheads). Cells are visualized under an Eclipse Ts2 Inverted Microscope (Nikon), using a 10x objective.

The epidermoid carcinoma A-431 cell line was used as a control line, in order to compare the phospholipid composition amongst different cell types. This cell line is derived from an 85-year old female and contains cancerous epithelial cells.

4.1.1 Cell Cultivation

Both cell lines were initially plated on 10 cm culture dishes before switching to 15 cm dishes as the cell count increased. For the 10 cm plates, cells were covered in 10 ml Dulbecco´s Modified Eagle´s Medium (DMEM, Sigma) high glucose, supplemented with 10% (v/v) fetal bovine serum (FBS, Sigma) and 1% (v/v) PenStrep (PS, Sigma) and left to grow in an incubator at 37°C supplied with 5% CO_2. Upon reaching a confluency of approximately 80-90% after 2-4 days, cells were detached by means of trypsinization and sub-cultured at ratios ranging from 1:2-1:4, depending on cell growth. Prior to the trypsinization, the old medium was discarded, and cells were washed once with 1xPBS to remove traces of the medium (as DMEM deactivates trypsin). For the SH-SY5Y cell line, each 10 cm cell plate was incubated in 2 ml trypsin (diluted 1:2 in PBS) for roughly 5 minutes before the trypsin was deactivated by the addition of 4 ml medium. The same amounts were added to the A-431 cells, but due to their connective nature, these cells required 15 min of trypsin incubation in order to detach. For the 15 cm culturing dishes, the amount of growth medium and trypsin was increased to 20 ml and 4 ml, respectively.

To ensure healthy growth conditions, cells were handled and kept in a sterile environment and frequently examined under a light microscope to monitor growth and check for abnormalities. Additionally, growth medium was replaced every other day, in order to provide the cells with a constant supply of nutrients.

4.1.2 Cell Lysate Preparation for Lipidomic Analysis

While the cells were on ice, the medium was removed, and the cells were subsequently washed twice with cold 1xPBS. After this, ice-cold 1xPBS was added to the plates and the cells were harvested using a cell scraper and directly transferred to a 50 mL tube. The cells were then pellet by centrifugation at 900xg for 5 min. The resulting supernatant was discarded, and the cell pellet was resuspended with 1 mL of 1xPBS and lysed by adding 333 µL of 3xGCTU. The lysate was subsequently vortexed and stored at -80°C before being freeze-dried overnight and stored at -20°C until further use.

4.2 Senescence Assay

Cellular senescence was induced in the SH-SY5Y cell line by treating the cells with etoposide, a cytotoxic anticancer agent that induces DNA damage and consequently cellular senescence. Before treating the cell-quantities needed to prepare NMR and MS samples (ten confluent 15 cm plates) a low-scale senescence-assay was conducted, optimizing treatment conditions.

4.2.1 Induction of Senescence

Optimal treatment conditions were determined by testing different cell densities and drug concentrations in 24-well plates. Cell counts of 100 000, 150 000, 250 000 and 300 000 per well were seeded out and left to grow overnight at 37°C. Etoposide concentrations of 5 μM, 10 μM, 15 μM and 20 μM was then examined using the cell count that provided a confluency of 70-80 % after 24 hours.

Cellular senescence was induced by treating ten confluent cell plates (15cm) with 5 μM etoposide diluted in DMEM growth medium for 48 hours before replacing the drug with pure growth medium and leaving them to incubate at 37°C for seven days whilst developing a senescence phenotype. Growth medium was replaced every other day, and cell death and morphology were frequently monitored and documented under a TMS-F Microscope (Nikon).

4.2.2 Identification of Senescence: β-Galactosidase Staining

Prior to staining, etoposide-treated cells were carefully washed twice with pre-warmed D-PBS (PBS supplemented with magnesium and calcium to prevent cell detachment, as senescent cells do not adhere to surfaces as strongly as young cells) and fixated in 4% PFA for 15 min on a rocker. Fixed cells were then washed in pure PBS to remove remnants of salt crystals from the D-PBS, and thereafter incubated in Sen-B-Gal staining solution for 24 hours at 37°C, tightly wrapped in parafilm to prevent the CO_2 from reducing the PH of the staining solution. After 24 hours cells were examined under an Eclipse Ts2 Inverted Microscope, to check for β-Galactosidase activity, represented as blue colored cells.

For the low-scale establishing assay, cells were fixed and stained directly in the 24-well plates in which they were grown, whereas for the NMR and MS samples, staining was conducted on coverslips added to the 15 cm plates prior to cell cultivation, and used as a verification of senescence before proceeding with the experiment.

4.3 Lipid Isolation

4.3.1 Solvent Extraction of Lipid Fraction

Lipids were extracted from the freeze-dried cellular matter using a biphasic solvent system consisting of dichloromethane/methanol/water, a modified version of the traditional Bligh & Dyer method, which uses chloroform instead of dichloromethane[75]. The cause of this replacement was to minimize lipid degradation, a side effect of using chloroform as an organic solvent. Additionally, triethylammonium ions (TEAC) were added as a counter-ion to facilitate the migration of phospholipids into the organic phase.

First, the sample was dissolved and homogenized in 20 mL of an organic solvent mixture (dichloromethane/methanol/TEAC 3:1:0.0005, v/v/w, 75% 28% 25%) before being transferred to a glass flask for phase separation. Additional 20 mL of methanol was then added to improve the solubilization of membrane lipids by disrupting hydrogen bonding and electrostatic interactions between protein-lipids and lipid-lipids. By subsequently adding water (water/organic solvent 1:2), two phases were formed: one organic phase containing dichloromethane and one aqueous phase containing water and ethanol. Lipids were transferred into the organic phase by carefully shaking the solution whilst frequently draining out the gas developed during the process. Next, one uniform phase was made by adding 20 mL of methanol and again shaking the solution to solubilize additional lipids. After incubating the monophasic solution for 15 min, two phases were made by adding 20 mL of the organic solvent dichloromethane and collecting the lower organic phase containing the lipids in an Erlenmeyer flask. Several washing steps with dichloromethane was performed in order to transfer as many soluble non-lipid components to the aqueous phase as possible. Lastly, isopropanol was added to the collected organic phase to uniform the solution.

4.3.2 Solvent Removal: Rotavapor and Nitrogen Gas

Solvents used to extract the lipids were removed from the sample by evaporation, using a Rotavapor R-100 (Buchi). Evaporation was achieved by transferring the organic phase, collected from the extraction step, to a rotary evaporation flask kept under vacuum (500 mpa) in a water bath of 40°C. As the solvent vaporized, the pressure was gradually lowered manually, always keeping the solution right below boiling point. When the solution tolerated a pressure of 40 mpa, the rotavapor was set in an automatic mode at 40 mpa for 20 min, removing the last traces of fluid. After all the liquid had evaporated, the resulting lipid crystals were dissolved with a mixture of 1:3 dichloromethane/methanol and transferred to a small vial (4 ml) for the NMR sample. 100 µl of this solution was transferred to another vial, for the LC-MS/MS analysis. Both vials were then kept under a continuous stream of nitrogen gas, to remove the solvents, and thereafter stored at -20°C until further use.

4.4 ^{31}P NMR

4.4.1 ^{31}P NMR sample Preparation

Prior to resuspension, the frozen lipid films were thawed at room temperature to avoid any water contamination in the sample. Afterwards the dried lipids were dissolved in 650 µL CUBO solution (supplemented with TMP) and transferred to an Eppendorf tube. Salts and other cellular debris were removed by centrifugation at 15200xg for 2 min, and the supernatant containing the lipids was transferred to an NMR glass tube. More CUBO was added to the NMR tube if needed, to compensate for insufficient amounts of supernatant. The NMR tube was immediately placed in the NMR machine for analysis. Four individual experiments were analyzed for the untreated cells, and three for the senescence-induced cells. CUBO was used as a solvent for all NMR experiments due to its good chemical shift reproducibility and chemical stability when working with phospholipids[84,85].

4.4.2 Solution-Phase ^{31}P NMR

Bruker BioSpin NEO600 spectrometer, equipped with a cryogenic probe operating at 300 K, was used to collect compositional information about the lipid isolates. The pulse program used was "zgig" and "DQD" was the acquisition mode. A list of the most important parameters used to obtain the ^{31}P NMR spectra are presented in table 4.4.2.

Table 4.4.2 – List of ^{31}P NMR parameters used in this study

Parameter	Value	Description
Size of fid (TD)	32768 Hz	Number of points to be digitalized.
Number of scans (NS)	2560	Several scans are carried out to improve the quality of the spectrum.
Spectral width	54.1617 ppm, 13157.895 Hz	A measure of the width of the frequency spectrum to be analyzed. Signals whose frequency falls within the spectral width will be detected.
Acquisition time	1.2451839 sec	The time needed to acquire one scan.
Duration of ^{31}P pulse (P1)	40 μsec	
Power level for P1 pulse	17.342 watts	
Recycling delay	8 sec	To insure relaxation of the ^{31}P nuclei between scans.
Dwell time (DW)	38.00 μsec	The delay before data acquisition after pulse.
Receiver gain (RG)	101	Digital amplification of signal.

4.4.3 ^{31}P NMR Spectral Processing

To analyze the data obtained from the solution-phase ^{31}P NMR, a software termed TopSpin 4.0.7 (Bruker) were utilized. The main goal was to determine the relative concentration of the individual lipids by comparing their signal integrals with one another, allowing for accurate ratio determination. Before assigning phospholipids to the detected peaks and determining their relative abundance, several spectral processing steps were conducted. First, automatic phase correction was applied, which is the process of adjusting the shape of the peaks, so they all have an absorptive, positive line-shape[86]. Next, the baseline was brought to zero by applying a 5-degree polynomial baseline correction. The spectra were then calibrated by setting PC, the highest abundant signal, to 0 ppm. Afterwards, all identified peaks were manually picked and deconvoluted, which is the process of decomposing peaks that overlap in order to extract information about "hidden peaks" (Figure 4.4.3). A list containing the ppms of all picked peaks, as well as their signal areal, were then extracted from TopSpin and processed further in Microsoft Excel to calculate the abundance of each lipid. Peak assignment was done by comparing identified values with previously published work[87-89].

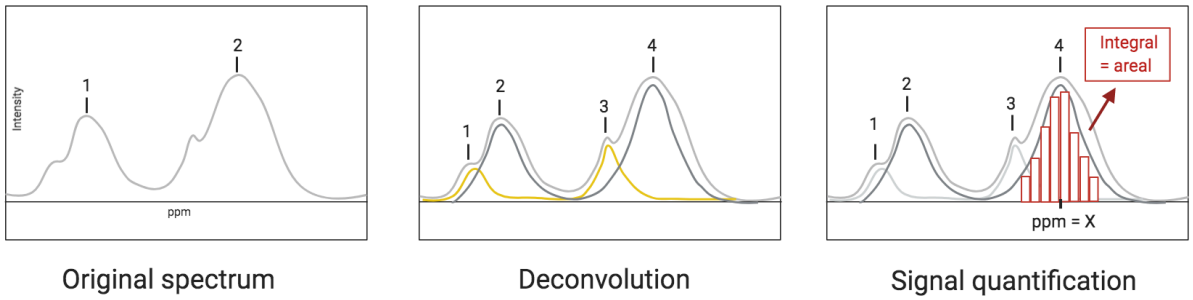

Figure 4.4.3 – NMR spectral deconvolution and integration. Deconvolution of the spectra is performed to identify the presence of hidden peaks (yellow)**.** Integrals of each peak area are then calculated to determine the relative abundance of the individual peaks/lipids. The illustration is created at Biorender.com.

4.5 LC-MS/MS

4.5.1 LC-MS/MS Sample Preparation

The combination of liquid chromatography (LC) and tandem mass spectrometry (MS/MS) was achieved using a Dionex Ultimate 3000 UPLC coupled with a Thermo Q-Exactive mass spectrometer (Thermo Fisher, USA). Before analyzing the structural identity of the individual components with MS/MS, LC was performed to separate the multiple components in the

mixture. LC conditions were set according to previously published work[88], and was aimed to elute the phospholipids as narrow peaks.

Dry lipid films were dissolved in a mixture of water, dichloromethane and acetonitrile (2:2:1) with 10 mM ammonium acetate. Next, the analytes were separated by injecting 20 µL into a UPLC C18 column with 1.7 µm particle size, at 318 K at a rate of 0.4 mL/min. Mobile phase A consisted of 40% acetonitrile and 60% water and mobile phase B consisted of 10% acetonitrile and 90% isopropanol. To improve the analyte ionization and thus the separation and detection of lipids, 10 mM ammonium acetate was added to both phases. A multistep gradient from 40 to 100% of solvent B was then used to separate the lipids. Lipid detection and identification was then achieved with MS/MS by monitoring the ions in scan ranges of 300-2000 m/z with a resolution of 140.000 at m/z = 200. Peaks detected in MS1 were fragmented for the second MS detector (MS2) using a collision energy of 24. The MS2 spectrum was collected with a resolution of 17,500 at m/z = 200 and an isolation window of 0.4 m/z, with the dynamic exclusion parameter set to "auto".

To ensure the detection of all lipid species occurring at the same retention time, an iterative exclusion (IE) protocol was utilized, which involved running each sample 3 times. Four independent experiments were analyzed for the untreated cells, whereas only one experiment was analyzed for the senescence-induced cells due to time restrictions (two more samples were isolated and ready to be analyzed but remained in the freezer due COVID-19-shutdown).

4.5.2 LC-MS/MS Data Processing

In order to analyze the amount of data obtained from LC-MS/MS, a script developed by Martin Jakubec *et al.,* referred to as the "LipMat script", was utilized[88]. LipMat was made in Matlab 2017b and comprises a library of lipid species and predicted lipid fragmentation patterns (see section 1.4.3 for more background information about LC-MS/MS and scripts). Generated LipMat-outputs included (i) a table of identified lipid species with their representative total score (S_{total}) and their retention time, (ii) MS2 fragmentation spectra with identified fragments highlighted in red, and (iii) chromatogram plots of the most abundant lipid species within each lipid head group.

Using LipMat, intact ion masses from MS1 were compared with the lipid library and in the case of a match, the MS2 spectrum of this hit were loaded and evaluated by the script to confirm the identity of the lipid. To achieve this confirmation, the MS2 spectra of each hit were given a score based on the presence of corresponding fragments and their intensity (S_{total}). As a result, LipMat generated a list of identified lipid species as well as their scoring. This list was then manually evaluated and only lipid species with a total score above 20 was processed further. For most lipids, the presence of both FA-chains (FA1 and FA2) was also needed for lipid conformation. One exception was SM, which only has one FA chain. All lipid species that did not meet these requirements, was excluded from further processing. Relative abundance of FAs within each head group was then calculated from the confirmed lipids and presented in bar charts. A schematic overview of the LC-MS/MS data processing steps are presented in Figure 4.5.2.

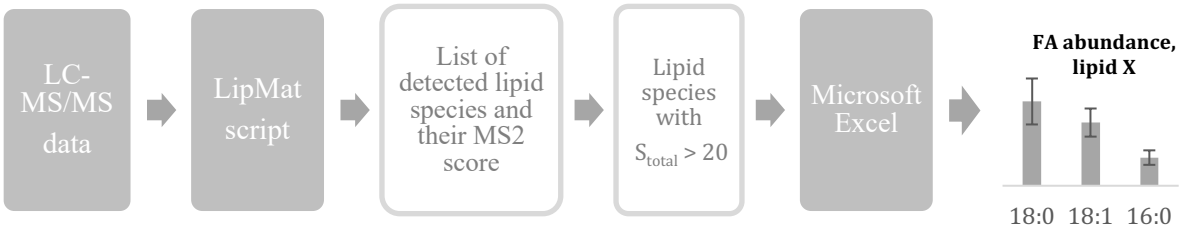

Figure 4.5.2 - Schematic overview of LC-MS/MS data processing. Experimental data from LC-MS/MS are processed using the LipMat script[88], which compares intact ion masses from MS1 with a lipid library. MS2 spectrum of hits are then loaded and scored based on the presence of corresponding lipid fragments[88]. LipMat generates a list of identified lipid species and their scoring which are then manually evaluated. Hits with sufficient score value and detected fragments (Fa1 and Fa2) are then further processed in Microsoft Excel, where bar charts of the most abundant fatty acid chains within each lipid head group are created.

5. RESULTS

5.1 Induction of Senescence

The hypothesis of this thesis is that age-related changes to the lipid composition of neuronal cells contributes to the misfolding process of α-Syn, leading to the harmful aggregates associated with PD. In order to test this hypothesis, cellular senescence was induced in the SH-SY5Y neuroblastoma cell line by treating cells with the cytotoxic anticancer agent etoposide. Finding the proper cell density prior to treating cells with etoposide was important as cells with too low confluency could risk not managing the toxic effect of the drug, resulting in massive cell death. On the other hand, over-confluency could result in reduced toxicity of the cytotoxic drug and false-positives in the senescence-confirmation assay (section 4.2.3). An optimal amount of etoposide was a drug concentration that affected as many cells as possible whilst keeping a low death rate. To determine optimal treatment conditions, various cell densities and drug concentrations were tested in 24-well plates, including a DMSO control.

Concerning cell density, wells containing 200 000 cells and above (250 000, 300 000), were over-confluent after 24 hours. The well containing 150 000 cells, on the other hand, revealed a confluency of 70-80% after 24 hours, a more appropriate density for further treatment. Thus, this cell seeding amount was therefore used for further experiments. Drug concentrations of 5 μM, 10 μM, 15 μM and 20 μM were tested on wells of 70-80% confluency and senescent cells were identified with the β-Galactosidase Staining assay (section 4.2.2). As seen in Figure 5.1.1 blue colored cells appeared at all drug concentrations, indicating ß-Galactosidase activity at pH 6 and thus a successful induction of senescence. In contrast, only a few blue cells were visible in the control plates, possibly due to over-confluency and not cellular senescence. At a drug concentration of 5 μM, most cells were affected whilst still being viable, contrary to cells treated with drug concentrations of 15 μM and 20 μM, where major cell losses were observed. Based on this, optimal treatment conditions were to treat cells of 70-80% confluency with a drug concentration of 5 μM.

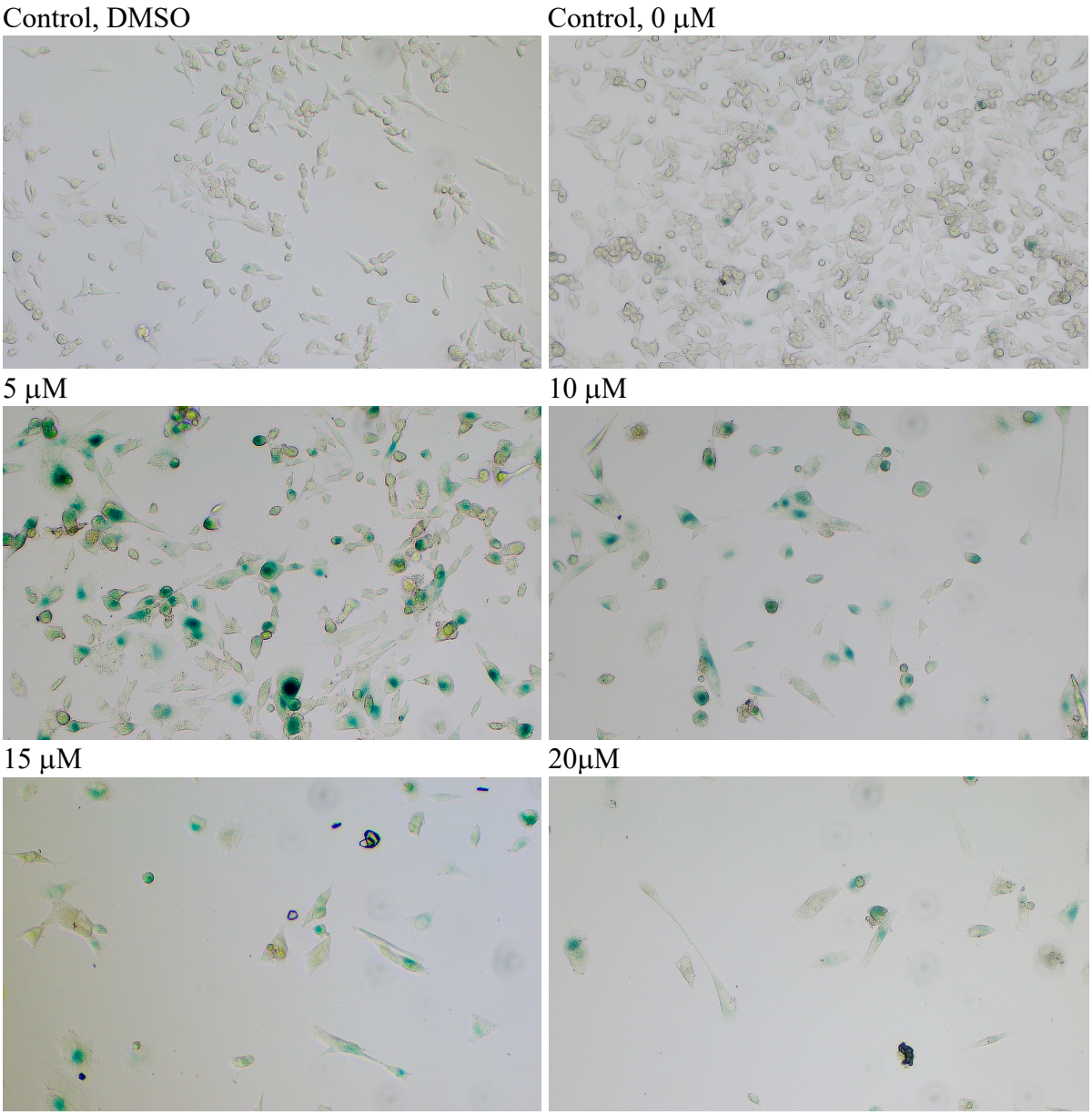

Figure 5.1.1 - Senescence-associated β-galactosidase activity in SH-SY5Y cells after treatment with etoposide. Cells of 70-80 % confluency were incubated with various drug concentrations (5, 10, 15 and 20 µM of etoposide diluted in DMSO) for 48h followed by further 7 days of incubation in fresh growth medium (DMEM, high glucose). X-gal was used for staining and β-galactosidase activity (represented as blue colored cells) was detected at pH 6 under an Eclipse Ts2 Inverted Microscope (Nikon), using an objective of 10x magnitude. Enzyme activity was detected at all drug concentrations, with the 5 µM having the lowest cell-death counts.

Figure 5.1.2 illustrates the changes in morphology between the untreated and etoposide-treated SH-SY5Y cells (day 7 after removing the drug). Looking at morphology of the neuron-like cells, the treated cells revealed a 2.5-fold increase in cell length compared to the untreated cells (calculated by ImageJ). Additionally, treated cells displayed a more

outstretched, irregular shape in contrast to their untreated counterparts, indicating a state of cellular senescence.

A) Untreated

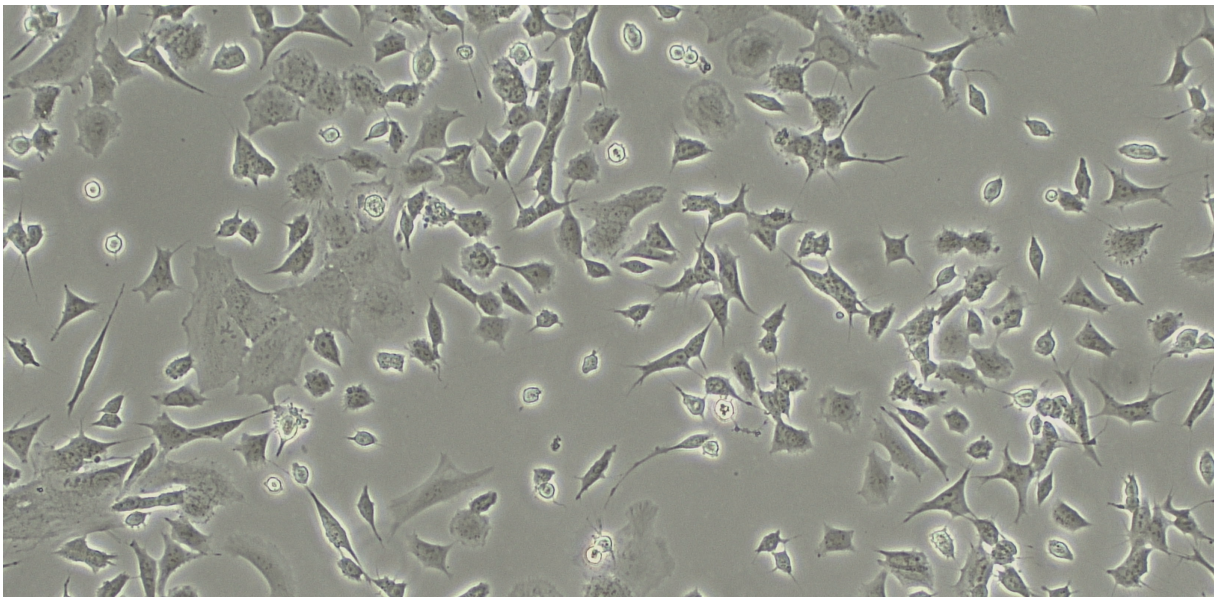

B) Etoposide-treated

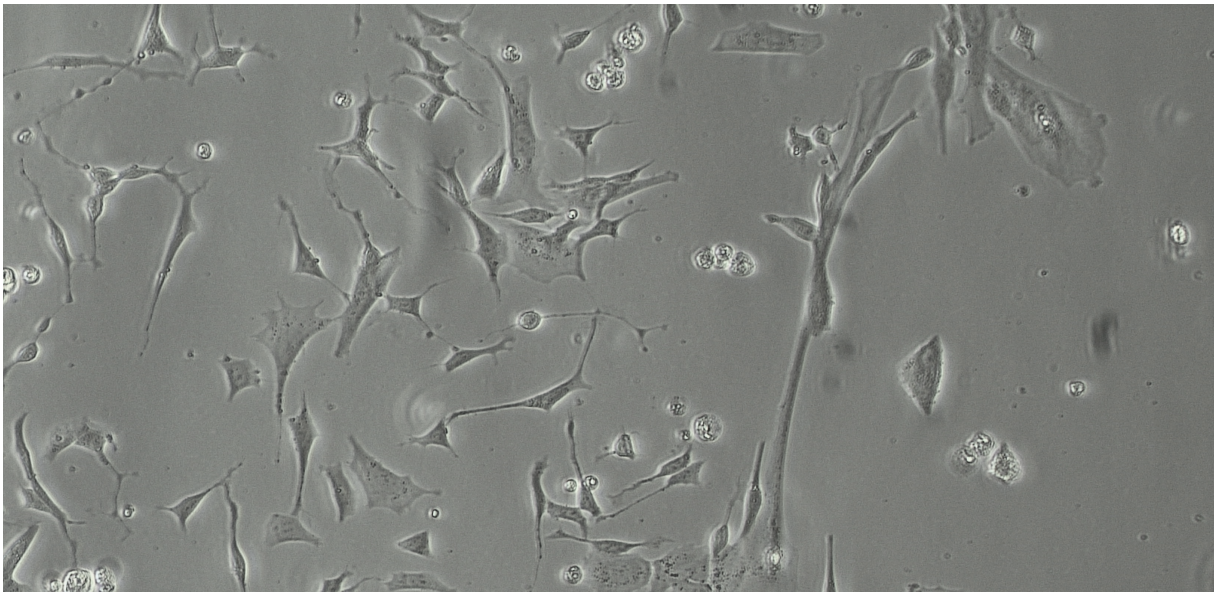

Figure 5.1.2 - Changes in cell morphology of etoposide-induced SH-SY5Y cells. A) Untreated cells of 70-80% confluency. B) Cells treated with 5 μM etoposide on day 7 after removing the drug. When comparing the neuron-like cell between the cell cultures, a 2.5-fold increase in length was measured for the treated cells using ImageJ. These cells also revealed a more irregular shape compared to the untreated cells, indicating the development of a senescent phenotype. Both pictures are taken under an Eclipse Ts2 Inverted Microscope (Nikon), with a 10x objective.

5.2 Lipid Identification and Quantification by ^{31}P NMR

^{31}P NMR was used for the identification and quantification of the various phospholipids present in the cell samples (see section 4.4.1 - 4.4.3 for experimental details). As only compounds containing phosphorus are detectable in the ^{31}P NMR spectrum, this method eliminates the disturbance of signals from other lipids. For this experiment, CUBO solvent was used to dissolve the lipids, due to its ability to spread the phospholipid resonances over a broad range of ppm while keeping linewidths at a minimum[85 84]. For each sample, data was acquired using a BioSpin NEO600 Spectrometer (Bruker), fitted with a probe able to detect signals from the ^{31}P nucleus. The ^{31}P NMR-data was processed in TopSpin 4.0.7 (Bruker) and lipid assignment was accomplished by comparing detected ppm with previously published work[88,90].

5.2.1 Lipid Composition of Untreated and Senescence-Induced SH-SY5Y Cells

For the SH-SY5Y cell line, ^{31}P NMR was performed on lipid isolates from untreated and etoposide-treated cells. Phospholipids detected and identified from one of the untreated SH-SY5Y lipid isolates are presented in Figure 5.2.1a, panel A. The spectra revealed a broad range of phospholipids occurring with different intensities, including PC, PS, PE, CL, SM, PI and PG as well as two low intensity PA-signals at around 5 ppm, indicating minimal sample degradation - as lipids often are reduced to their PA precursor when exposed to various degradation processes. Among these, the PC signal was the most prominent, and was used to calibrate the ^{31}P chemical shift scale (this signal was set to 0 ppm). The spectra also revealed a high peak at around 2.5 ppm, representing the phosphorus probe molecule (TMP) added to the CUBO solvent solution. This very large signal may have disturbed the other signals and perturbed the spectrum slightly, as most of the lipids had ppm values a little above their literature values. In order to perform a statistical comparison between different sets of samples, four biological replicates were prepared, acquired on, and analyzed (see supplementary 8.1 for spectra of all replicates).

One of the ^{31}P NMR spectra of phospholipids identified in the senescence-induced SH-SY5Y cells are shown in Figure 5.2.1a, panel B. The same range of phospholipids as for the untreated samples, were detected in these samples, as well as a low PA-signal at 5 ppm indicating minimal sample degradation. Unlike the untreated samples, no signal for PG was

visible in the senescence-induced ones. The signal for TMP (ppm 2.5) was much less dominant in these samples, which was made with an older CUBO solution containing a lower TMP concentration. For these cells, lipid analysis was performed on lipid isolates from three independent experiments (see supplementary 8.2 for all spectra).

A) Untreated SH-SY5Y cells

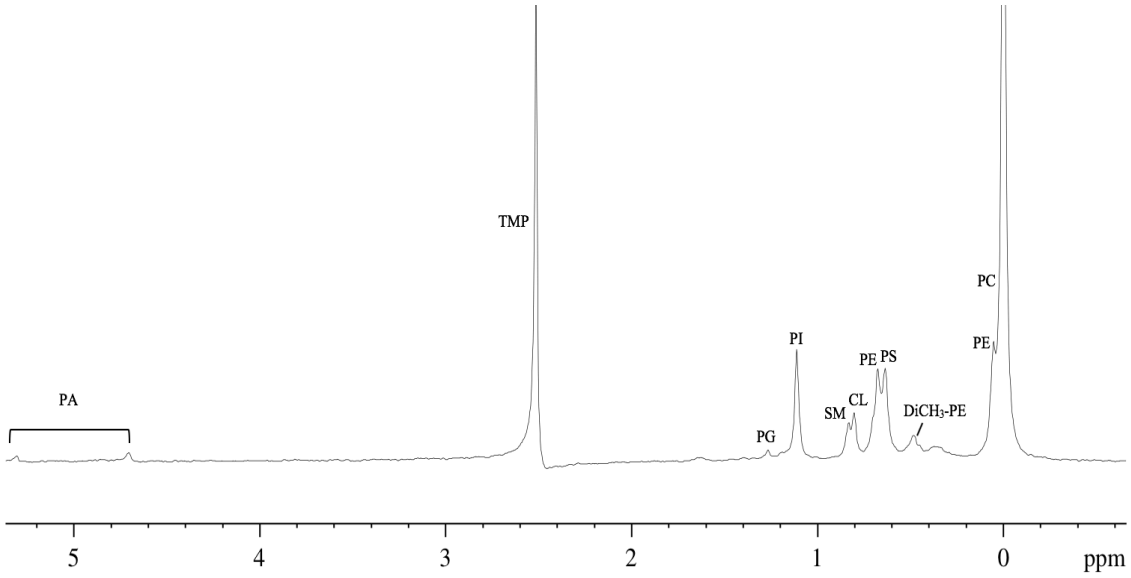

B) Senescence-induced SH-SY5Y cells

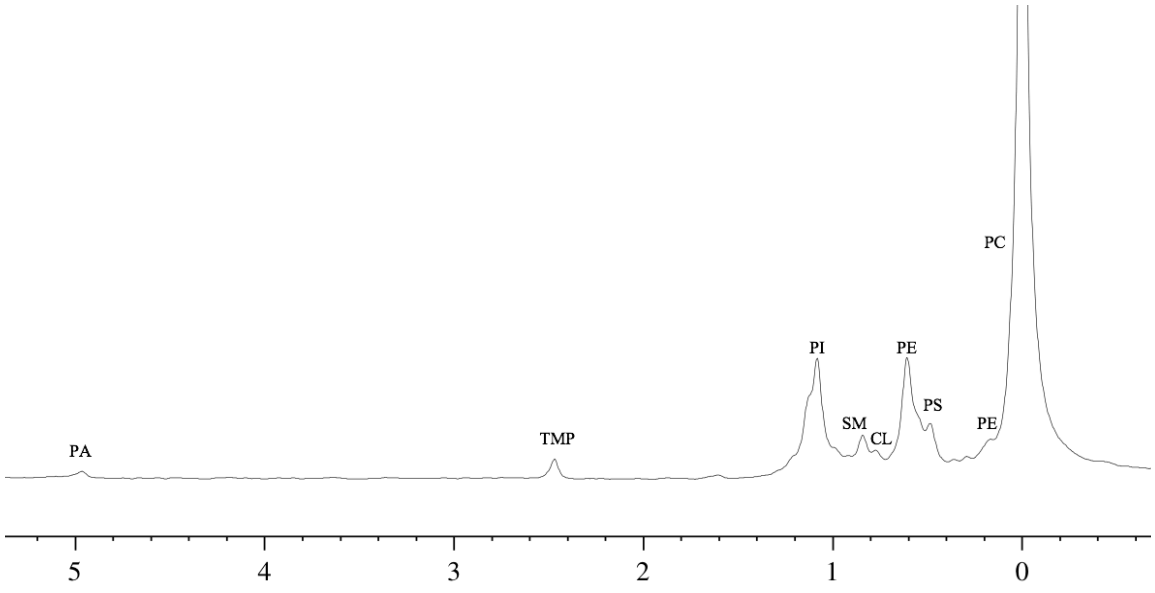

Figure 5.2.1a – Representative ^{31}P NMR spectra of phospholipid composition. Two ^{31}P NMR spectra are depicted in the figure, presenting the phospholipid composition in (A) untreated and (B) senescence-induced SH-SY5Y cells. Cellular senescence was induced with 5 μM etoposide. In both cases, PC (the highest abundant lipid) was used to calibrate the axis (set to 0 ppm). PA, phosphatic acid; PC, phosphatidylcholine; PE, phosphatidylethanolamine; PG, phosphatidylglycerol; PI, phosphatidylinositol; PS, phosphatidylserine; SM, sphingomyelin; CL, cardiolipin.

A bar chart comparing the relative abundances of phospholipids in the untreated and senescence-induced samples are presented in Figure 5.2.1b. For both samples, the most abundant lipid species by far were PC lipids, with a total abundance of 49 ± 4.7% for the untreated and 57.6 ± 9.1% for the senescence-induced cells. In the untreated sample, the second most abundant lipid was PE (19.8 ± 5.2%), followed by PI (8.0 ± 1.6%). For the senescence-induced cells, this order was the opposite with PI being the second most abundant lipid of 12.7 ± 3.6% abundance, followed by PE (12.3 ± 7.5%). When comparing the samples, a significant reduction of 58% (Welch t-test, $p = 0.02$) was detected in the senescent cell's abundance of SM. Although not significant, the results also indicated a senescence-related increase in abundance of the negatively charged lipids PI and PS of 37% (Welch t-test, $p = 0.12$) and 19% (Welch t-test, $p = 0.75$), respectively. No signal for PG was detected in the senescence-induced cells. However, it is worth mentioning that NMR suffers from lack of sensitivity when little sample material is available, so it is possible that PG was present in the sample but in too low quantities to be detected. Seeing as etoposide is toxic for the cells, some cells probably died during the culturing process, leaving less material available for the NMR.

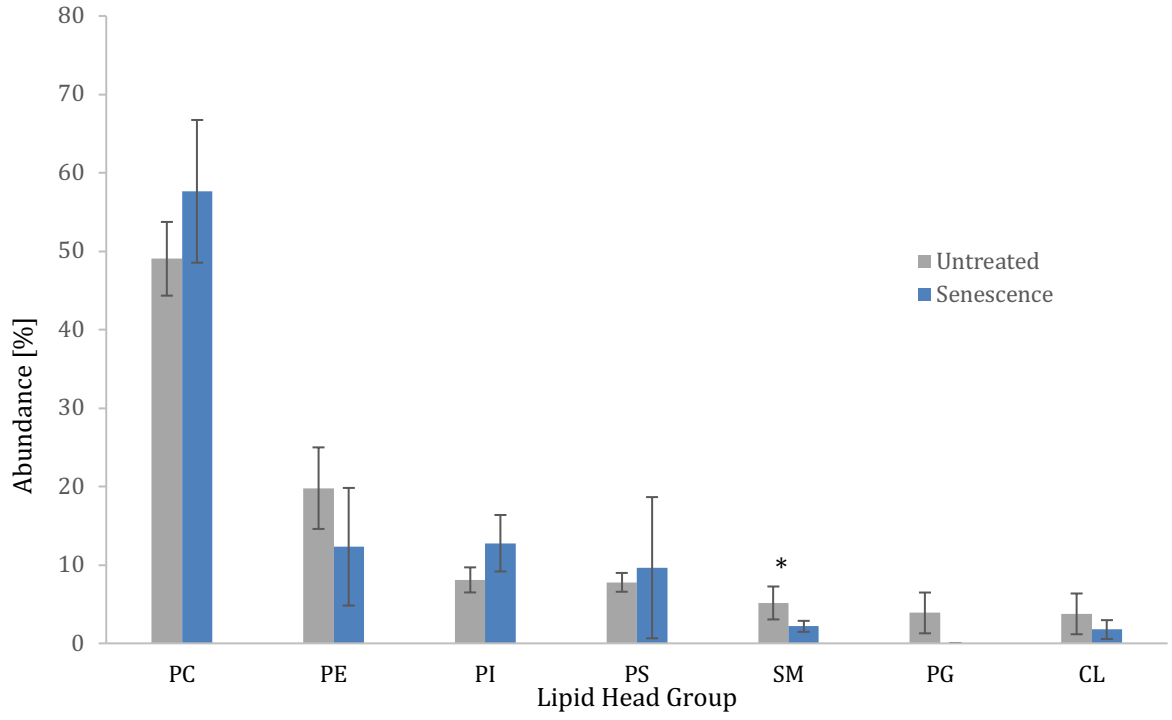

Figure 5.2.1b - Abundance of phospholipids identified in SH-SY5Y lipid isolates. ^{31}P NMR was used to profile phospholipids extracted from untreated (grey) and senescent-induced (blue) SH-SY5Y cells. For both samples the most abundant lipid was PC. A statistical hypothesis test (Welch's t-test) found a significant decrease of 58% ($p = 0.02$*) in the abundance of SM, when comparing the two samples. Results from both the untreated and senescence-induced sample are representative of four biological replicates.

5.2.2 Lipid Composition of A-431 Cells

As previous studies have discovered that the phospholipid composition of lipid membranes differs between cell types[91], an epithelial A-431 cell line was used as a comparable control to the neuroblastoma SH-SY5Y cell line. Phospholipids detected and identified in the A-431 lipid isolates are presented in a ^{31}P NMR spectrum (Figure 5.2.2a). The same phospholipids as for the SH-SY5Y cell line were identified also in this cell line, but at slightly different intensities. In addition to these, an unidentified signal was detected at 3.1 ppm, accounting for 4.3% of the total lipid abundance. Unfortunately, due to time limitations, only one A-431 sample was analyzed with ^{31}P NMR.

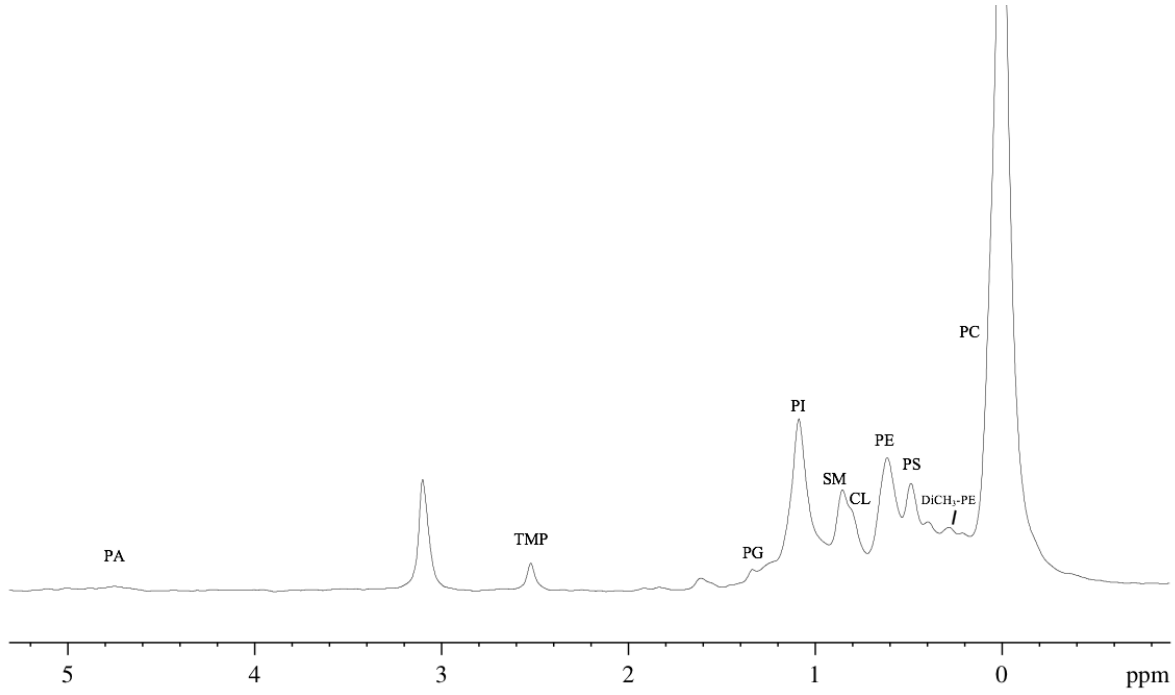

Figure 5.2.2a – Representative ^{31}P NMR spectrum of phospholipid composition in A-431 cells. Lipid assignment was done after deconvolution of the spectrum, and the PC signal (the highest abundant lipid) was used to calibrate the axis (set to 0 ppm). PA, phosphatic acid; PC, phosphatidylcholine; PE, phosphatidylethanolamine; PG, phosphatidylglycerol; PI, phosphatidylinositol; PS, phosphatidylserine; SM, sphingomyelin; CL, cardiolipin.

A bar chart comparing the total abundance of phospholipids identified in the A-431 and SH-SY5Y cells are presented in Figure 5.2.2b. In the A-431 cells, the most abundant lipid, PC, accounted for 57.7% of total abundance, followed by PI (12.5%) and PE (10.5%). The least abundant lipids were PG and CL with a total abundance of 0.3% and 1%, respectively, which constitutes a decrease of 92.8% and 73.7% when comparing to the PG and CL content detected in the SH-SY5Y cell line. The same was observed with PE, which revealed a reduction of 47.0%. PI and PC abundance on the other hand, were 54.5% and 17.6% higher in the A-431 cell line compared to the SH-SY5Y cells. For SM, no major differences were observed amongst the two samples.

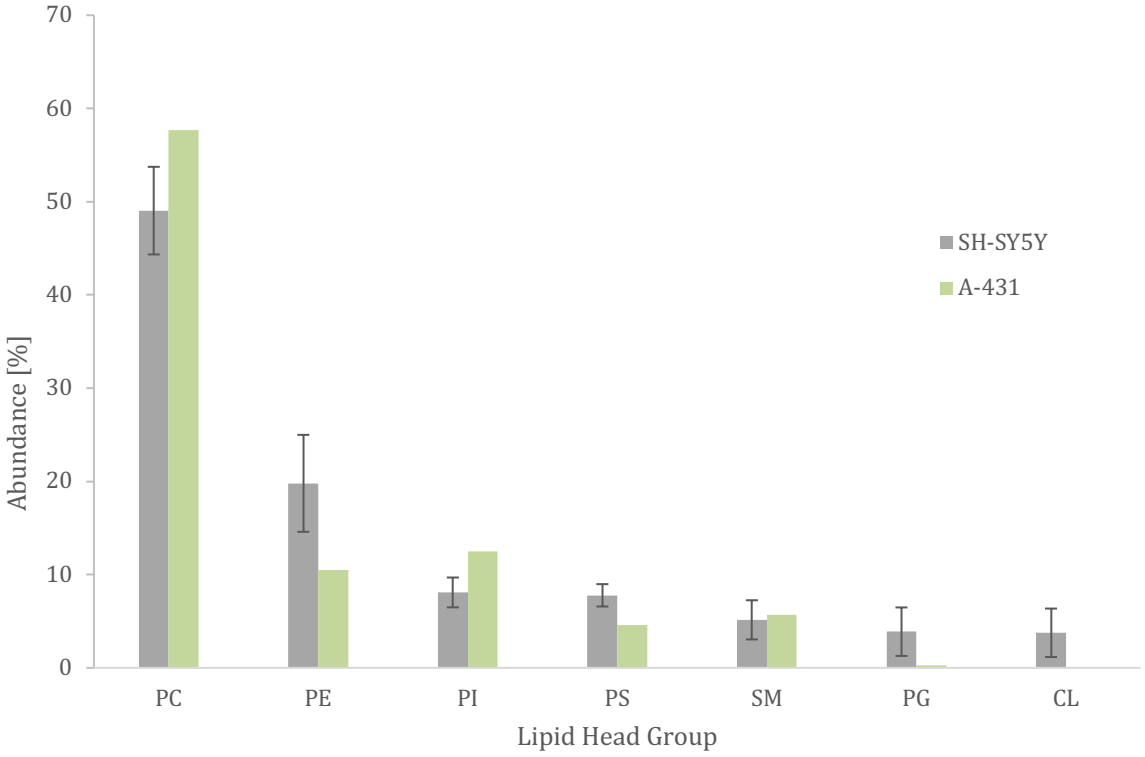

Figure 5.2.2b - Abundance of phospholipids identified in A-431 and SH-SY5Y lipid isolates. Each column represents the relative abundance of an individual phospholipid detected with ^{31}P NMR. Phospholipid composition of A-431 cells (green) are aligned with the composition of SH-SY5Y cells (grey), for comparison. For the latter, the bars are representative of four independent experiments, whereas only one experiment was made with the A-431 cells due to time limitations. PC, phosphatidylcholine; PE, phosphatidylethanolamine; PG, phosphatidylglycerol; PI, phosphatidylinositol; PS, phosphatidylserine; SM, sphingomyelin; CL, cardiolipin.

5.3 Fatty Acid Analysis by LC-MS/MS

More information about the lipids, including their FA sidechains and the range of lipid isoforms present, was acquired with LC-MS/MS. Data were processed using a script called the LipMat[88] script, and only lipids species with a $S_{total} > 20$ was included. Unfortunately, as only one replicate of the senescence-induced cells was analyzed with LC-MS/MS, no statistical analysis could be performed when comparing these samples.

5.3.1 Fatty Acid Composition in Untreated SH-SY5Y Cells

An example of a LC-chromatogram LipMat-output are presented in Figure 5.3.1a, panel A. The chromatogram shows the five most abundant PC lipid species identified in one of the untreated SH-SY5Y samples. The area for each lipid is plotted against the retention time. At the top is "PC-CH_3CO_2 16:0/18:1" which had the highest signal among the PC lipid species, thus were the most abundant. Panel B shows the MS2 spectrum of "PC-CH_3CO_2 16:0/18:1". Looking at the spectrum, both FAs were identified, in addition to a fragment at 462.3 m/z – representing a demethylated FA2. The MS2 spectrum were given total score of 40.7 (S_{total}), well above the 20-limit set for confirmation.

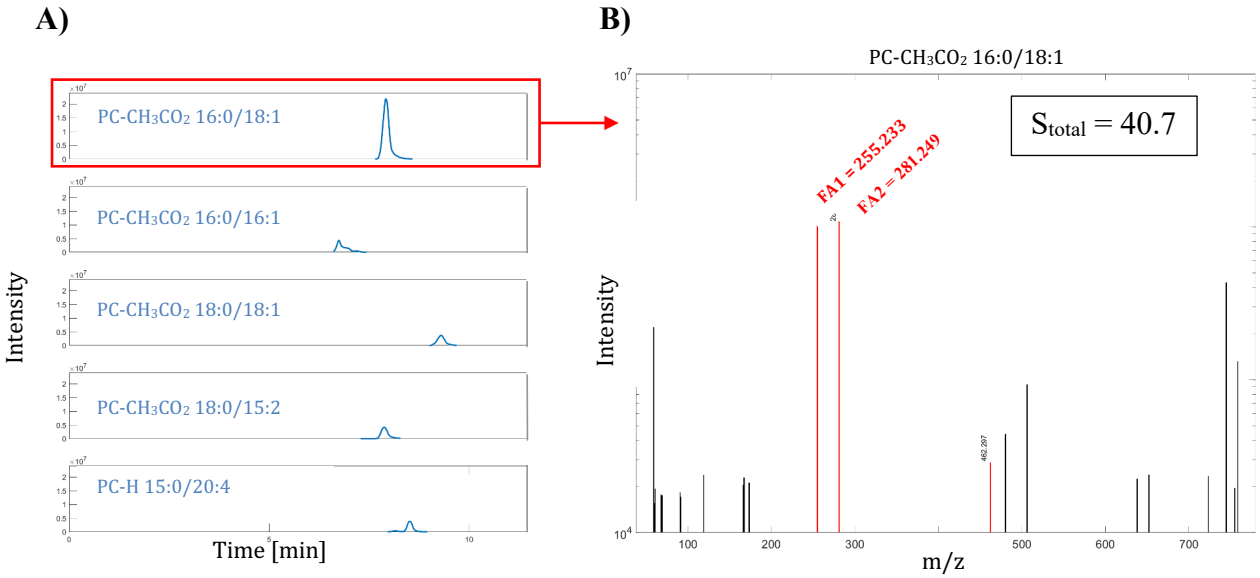

Figure 5.3.1a – LC-MS/MS analysis of SH-SY5Y lipid isolates. A) Example of a LC-chromatogram output showing the five most abundant lipid species for PC. The signal intensity (y-axis) of each molecule is plotted against their retention time (x-axis, min). B) MS2 spectrum of the most abundant PC species "PC-CH3CO2 16:0/18:1". The spectrum shows the MS2 fragmentation pattern of the molecule, and identified fragments are highlighted in red. Based on this lipid's intensity and MS2 spectrum, MatLab calculated a $S_{total} = 40.7$ for this hit.

Representative bar charts showing the most abundant FA chains within PC, PI, SM, PE, PG and PS, from the untreated SH-SY5Y-sample, are presented in Figure 5.3.1b. Concerning CL, LC-MS/MS did not detect enough FA chains to present a plot. In most of the lipid head groups presented, the most abundant FA chains included stearic acid (18:0), palmitic acid (16:0) as well as their monounsaturated derivatives oleic acid (18:1) and palmitoleic acid (16:1). In PG, the polyunsaturated omega-6 fatty acid arachidonic acid (ARA, 20:4) was the most abundant of all, accounting for 27.1± 7.9% of the total FA content. For SM, the only FAs occurring in all four samples, were 16:1 and 18:0, which were distributed 50:50 in all the detected lipids. A total of 84, 116, 154, 94 lipid species were confirmed in the four individual experiments.

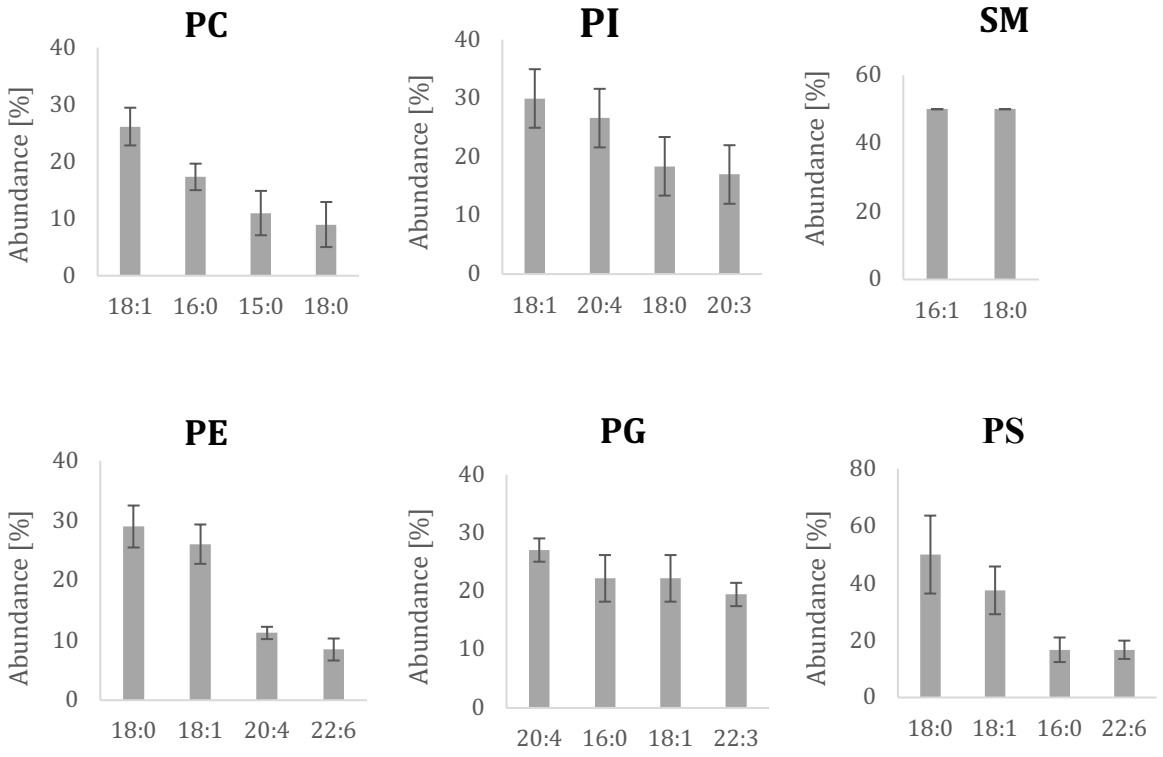

Figure 5.3.1b – Fatty acid distribution within lipid head groups in SH-SY5Y cells. The individual bar charts represent the most abundant FA chains within PC, PI, SM, PE, PG and PS, detected with MS/MS and evaluated using the LipMat script[88]. For cardiolipin (CL), there was insufficient amount of identified FA chains to be presented. PC, phosphatidylcholine; PE, phosphatidylethanolamine; PG, phosphatidylglycerol; PI, phosphatidylinositol; PS, phosphatidylserine; SM, sphingomyelin.

5.3.2 Fatty Acid Composition in Senescence-induced SH-SY5Y Cells

Graphical representation of the LC-MS/MS analysis, showing the FA abundance in the senescence-induced SH-SY5Y cells, are presented in Figure 5.3.2. Similar to the untreated cells, the most abundant FA chains in most of the lipid head groups included 18:0, 16:0, 18:1 and 16:1. There was, on the other hand, a higher proportion of the monounsaturated form of the mentioned FAs in the senescence-induced cells, with 18:1 being the overall most abundant FA in both PC, PE, PG and PS. Thus, in PG, 20:4 (12.5%) was replaced with 18:1 (29.2%) for the most abundant FAs. A total of 318 confirmed lipid species were detected for this sample.

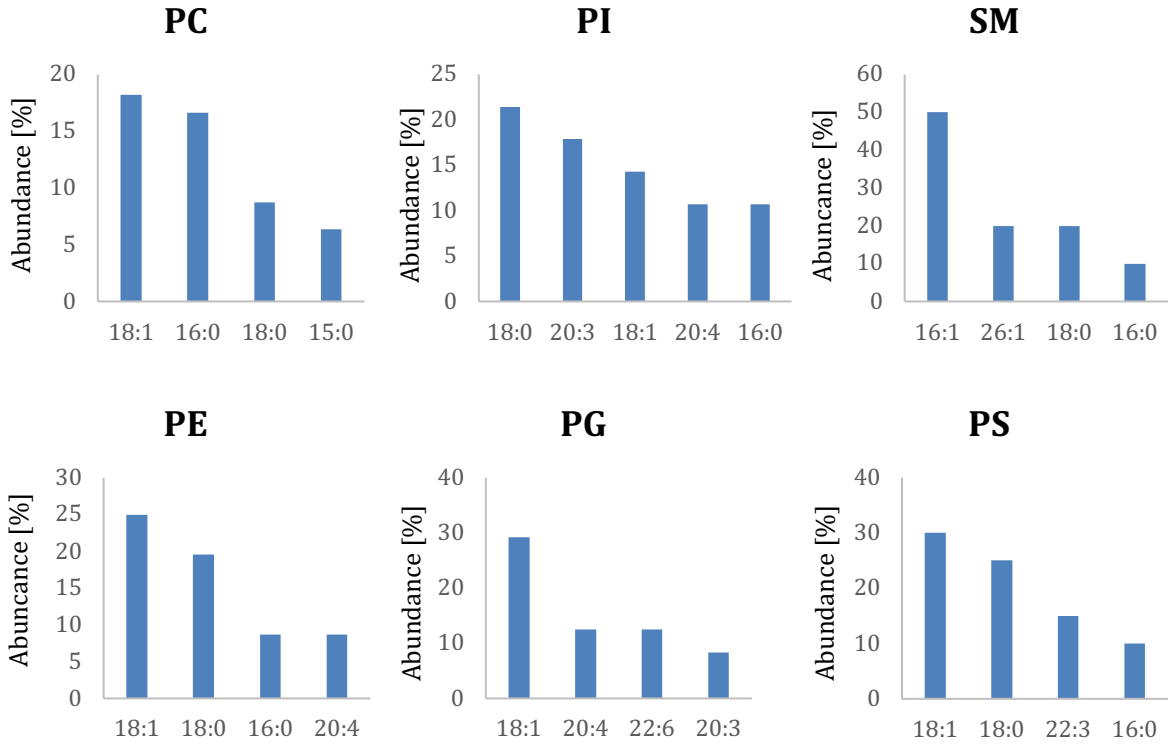

Figure 5.3.2 –Fatty acid distribution within lipid head groups in senescence-induced SH-SY5Y cells. Cellular senescence was induced in SH-SY5Y cells with etoposide (5µM) and information about the FA chains were detected using MS/MS and evaluated using the LipMat script developed by Martin Jakubec *et al*[88]. The most abundant FA chains within PC, PI, SM, PE, PG and PS are represented in individual bar charts. Concerning cardiolipin (CL), no FA scored above 20 in LipMat to present a plot. PC, phosphatidylcholine; PE, phosphatidylethanolamine; PG, phosphatidylglycerol; PI, phosphatidylinositol; PS, phosphatidylserine; SM, sphingomyelin.

5.3.3 Comparison of Degree of Saturation in Untreated and Senescence-induced Cells

When comparing the two cell samples, the senescence-induced cells revealed an overall decrease of 10.4 ± 2.6% in the abundance of PUFAs with a similar increase in MUFAs of 13.8 ± 1.2% (Figure 5.3.3a). No remarkable changes were observed in the total amount of SFAs, revealing a decrease of 2.5 ± 1.5 %.

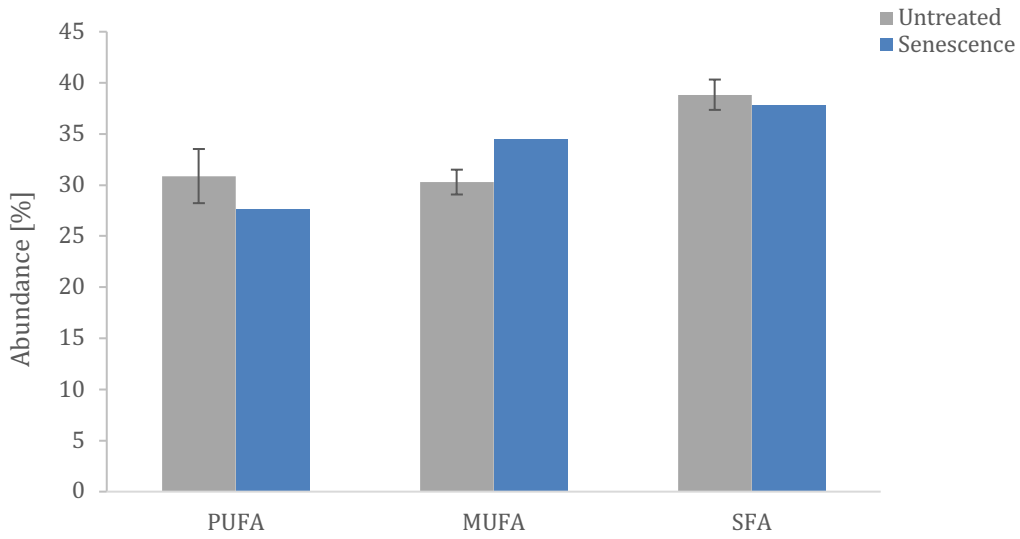

Figure 5.3.3a - Graphical comparison of PUFA, MUFA and SFA content in SH-SY5Y cells. Bar charts were constructed for visualizing the total amount of polyunsaturated (PUFA), monounsaturated (MUFA) and saturated (SFA) fatty acid (FA) sidechains in untreated (grey) and senescence-induced (blue) SH-SY5Y cells, after detection with MS/MS. In the senescence-induced sample, the plot reveals a reduction in PUFAs with an inversely correlated increase in MUFAs.

Two PUFAs implicated with aging is AA and DHA. Graphical comparison of their total abundance in the untreated and senescence-induced samples are presented in 5.3.3b, panel A. As shown in the figure, AA abundance were inversely correlated with cellular senescence, revealing a decrease of 45.8 ± 2.2%, whereas no remarkable difference was found in the DHA abundance. Looking closer at AA abundance, this FA revealed a decrease in all the lipid head groups it was identified in, including in PG (-57.7 ± 4.4%), PI (-63.3 ± 5.6%), PE (-22.6 ± 1.0%) and PC (-39.5 ± 2.1%) (Figure 5.3.3b, panel B).

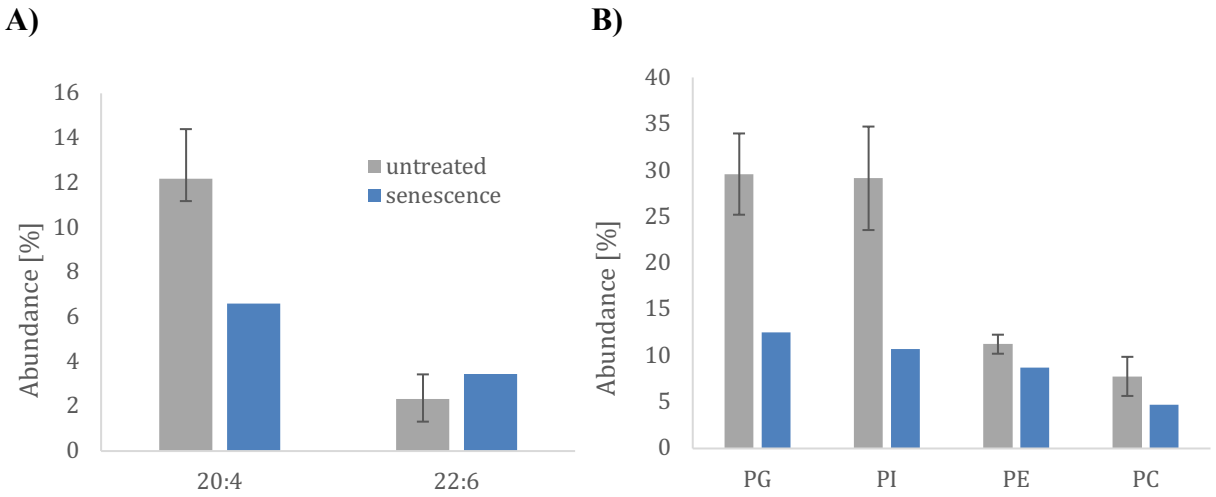

Figure 5.3.3b – AA and DHA abundance in senescence-induced SH-SY5Y cells. A) Comparison of 20:4 (arachidonic acid, AA) and 22:6 (docosahexaenoic acid, DHA) abundance in untreated (grey) and senescence-induced (blue) SH-SY5Y cells. B) Differences in AA abundance within phosphatidylglycerol (PG), phosphatidylinositol (PI), phosphatidylethanolamine (PE) and phosphatidylcholine (PC).

As mentioned in section 5.3.2 and visualized in Figure 5.3.2, the senescence-induced cells revealed an overall increase in the abundance of the monounsaturated acids 18:1 and 16:1 compared the saturated acids 18:0 and 16:0. A graphical comparison of the total abundance of these acids in the untreated and senescence-induced cells are presented in Figure 5.3.3c. Regarding the 18:0/18:1 ratio, the senescent cells revealed an ratio of 0.74 ± 0.11 compared to 0.63 in the senescence-induced cell, implying an increase of 14.0 ± 1.36% in the 18:1 content (Figure 5.3.3c, panel A). When comparing the 16:0/16:1 ratio, an increase of 64.7 ± 44.3% in the 16:1 content was observed.

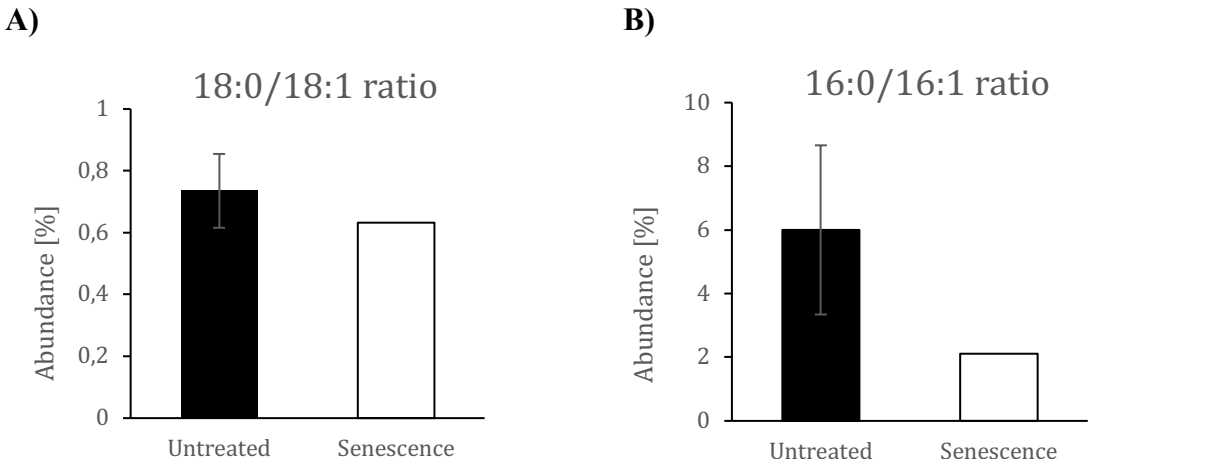

Figure 5.3.3c - 18:0/18:1 and 16:0/16:1 ratio in senescence-induced SH-SY5Y cells. A) Comparison of the 18:0/18:1 (stearic/oleic acid) ratio in untreated (black) and senescence-induced cells (white). B) 16:0/16:1 (palmitic/palmitoleic acid) ratio in untreated (black) and senescence-induced (white) cells. Both results (A, B) are a graphical representation of LC-MS/MS fatty acid analysis.

Graphical comparison of the abundance of various FA chain-lengths ranging from 10-24 carbon atoms, are presented in Figure 5.3.4. Most of the phospholipids in both samples contained FAs of 16-18 carbons of length, accounting for 64.0 ± 5.8% (untreated) and 59.4% (senescent) of the total FA content. When comparing the samples, no major differences was found between the abundance of the individual FA chain lengths. One exception was the abundance of FAs with chains between 10-12 of length, in which LC-MS/MS did not detect any species of this length in the untreated cells compared to 2.2% in the treated cells.

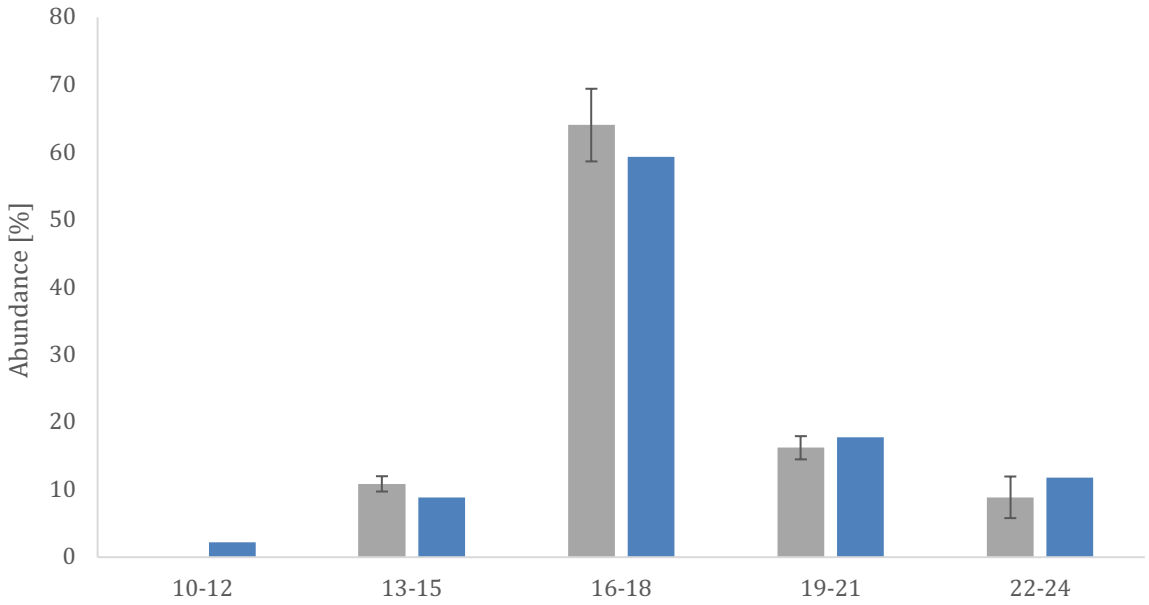

Figure 5.3.4 – Graphical comparison of fatty acid chain length abundance. Columns represents the abundance of fatty acid (FA) chains of 10-12, 13-15, 16-18, 19-21 and 22-24 carbons identified in untreated (grey) and senescence-induced (blue) SH-SY5Y cells using LC-MS/MS.

6. DISCUSSION

This thesis aimed to investigate age-related changes to the lipid composition of neurons in hopes of finding a correlation between the aging cell and the development of neurodegenerative disorders like PD. The choice of objective was based on the importance of aging in regard to the development of PD, combined with emerging studies connecting lipids to the aggregation process of α-Syn. In order to mimic old neurons, cellular senescence was induced to the neuroblastoma SH-SY5Y cell line using the cytotoxic anticancer agent etoposide. Confirmation of senescence was achieved with Senescence-associated β-Galactosidase Staining (SA-β-gal) and a combination of solution-phase ^{31}P NMR and LC-MS/MS was used for lipid profiling.

6.1 Cellular Senescence as a Model System for Aging

Based on the findings that cells induced with 5 μM etoposide revealed a 2.5 increase in length (Figure 5.1.2) as well as a high degree of ß-Galactosidase activity at pH 6 (Figure 5.1.1), it is reasonable to conclude that cellular senescence was successfully induced in the SH-SY5Y cell line. Another finding supporting this assumption was the 37% (Welch t-test, $p = 0.12$) increase of PI-content identified with ^{31}P NMR (5.2.1b). Phosphorylated forms of PI, called phosphoinositides, plays key roles in cell signaling e.g via the PI3K/AKT/mTOR pathway, an intracellular signaling pathway important in regulating the cell cycle[92]. Seeing as cellular senescence is dependent on signal transduction to initiate and maintain the cell cycle growth arrest, it is not unlikely that there is a connection between senescence and PI metabolism.

One of the assumptions for conducting the study was that cellular senescence could be used as a model system for aging. Seeing as neurons are non-dividing cells carrying important information for the individual, the only way to study age-related changes to these cells are to examine brains of deceased in which natural variations among the population as well as decomposing processes has to be taking into account. There seems, however, to be similarities between the aging process and the process of cellular senescence, suggesting the latter could be used a model system for aging. Indeed, by comparing the lipids from untreated SH-SY5Y cells with those induced with cellular senescence, several discoveries corresponding with literature about neuronal aging were made in this thesis.

Using ^{31}P NMR, a significant reduction of 58% (Welch t-test, p = 0.02*) in SM levels were detected in the senescent cells when comparing to the untreated ones (Figure 5.2.1b). Similar findings have been made by studying brain lipids of deceased individuals at age 20-100 years, in which SM revealed an almost twice as fast age-related decrease in abundance, compared to other lipids[93].

Additionally, by analyzing FA composition with LC-MS/MS, there was an overall decrease of 10.4% in the abundance of PUFAs, combined with a similar increase of 13.8% in MUFAs (Figure 5.3.3a). The levels of AA in particular, were altered in all the lipid head groups it was identified in, resulting in a total decrease of 45.8% (Figure 5.3.3b). Other LC-MS/MS observations made, were changes to the 18:0/18:1 acid ratio, where the untreated cells were more abundant in 18:0 compared to its monounsaturated derivate, whilst the opposite was observed in the senescent cells, which were more abundant in 18:1 (Figure 5.3.3c). Consistent with all of these results are FA analysis obtained from brain tissues of human subjects aged 29-80 years at time of death, published in a study by McNamara *et al*[61]. This study found that age inversely correlated with the amount of PUFAs, especially AA, simultaneously with an increase in stearoyl-CoA desaturase activity, resulting in elevated MUFAs levels. McNamara *et al*. also observed an age-related progressive decrease in the 18:0/18:1 acid ratio combined with an increase in stearoyl-CoA-desaturase (SCD) activity – the enzyme responsible for the conversion of 18:0 into 18:1. Altogether, these findings indicate a high degree of similarities between the aging cell and the state of cellular senescence, thus making it a suitable model system for neuronal aging.

6.2 Lipid Profile Comparison of the A-431 and SH-SY5Y Cell Lines

To find out if the lipid composition of DA neurons differed from that of other cell types, the epithelial A-431 cell line was used as a comparable control to the SH-SY5Y line. One interesting difference detected with ^{31}P NMR, was the 73.7% decrease in CL abundance in the A-431 cell line (Figure 5.2.2b) as CL is almost exclusively located in the inner mitochondrial membrane of cells[94]. Therefore, this result implies that the SH-SY5Y cells contain more mitochondria than the epithelial cells, thus making them particularly energetically active. Another result backing up this assumption is the 92.8% decrease in PG as it appears that the

primary role of PG in animal membranes is being a precursor for mitochondrial CL[95]. Based on the high energy requirements of the brain tissue (consuming 20% of the body's total oxygen), it makes perfect sense that brain cells are more enriched in mitochondria than epithelial cells. Nevertheless, these major differences may also reflect the cancerous origin of the neuroblastoma SH-SY5Y cell line, as mitochondrial biogenesis often is upregulated in cancers[96].

6.3 Findings with implications for Parkinson's disease

6.3.1 - Increase in PS and PI Content

In order to draw connections between the lipid composition of aged cells and the aggregation propensity of α-Syn, changes detected in the senescent cells have to be compared to literature about α-Syn binding and aggregation. Previous studies have observed that α-Syn preferably binds to membranes of a highly negatively charged lipid content. This knowledge is aligned with the ^{31}P NMR results in this thesis, as senescent cells revealed a 37% (Welch t-test, $p = 0.12$) and 19% (Welch t-test, $p = 0.75$) increase in the abundance of the negatively charged lipids PS and PI (Figure 5.2.1b). It is not certain that these negatively charged lipids directly affect the aggregation propensity or just the binding affinity. However, C. Galvagnion *et al*. did discover that at high lipid/protein ratios, the presence of negatively charged lipids increased the aggregation rate[41]. Seeing as aging generally increases the likelihood of mutations, it is reasonable to assume that aging also increases the possibility of mutations in genes implicated in PD, resulting in elevated α-Syn levels or a lack of being able to remove distorted proteins. Combined, the age-related elevation in α-Syn and PS/PI content could possibly affect the aggregation propensity of α-Syn.

6.3.2 – Decrease in PUFA Content

LC-MS/MS revealed an overall decrease of 10.4 ± 2.6% in the abundance of PUFA simultaneously with a 13.8 ± 1.2% increase in MUFAs (Figure 5.3.3a). This decrease in PUFA content may result in a more compact and less fluid membrane, which again can have implications for the development of PD as fluid membranes seem to play a key role in α-Syn

homeostasis by preventing the protein from aggregating [43]. Furthermore, these FAs do have important roles in brain health including regulation of cell survival, neurogenesis, brain inflammation, and synaptic function, suggesting that any compositional alterations may have implications for these functions[97]. Indeed, the beneficial effects of omega-3 PUFAs have been reported in a range of disorders of the nervous system. In one long-term clinical study, over 5000 subjects were evaluated for the risk of developing PD in relation to their dietary intake of FAs[31]. After 6 years, a correlation between high PUFA consumption and decreased risk of PD was observed, proposing low-PUFA intake as a potential risk factor for neurodegenerative disorders. Several other studies have come to the same conclusions[98], emphasizing the importance of diet in regard to lipid membrane composition and possibly the likelihood of developing neurodegenerative disorders.

6.3.3 - Decrease in the 18:0/18:1 Ratio

The senescence-related increase in MUFAs were reflected in the 14.0 ± 1.36% decrease in the treated cells 18:0/18:1 ratio. In the context of PD, this is yet another interesting finding as some researchers now claim that 18:1 may worsen α-Syn pathology by causing aggregates of the protein to build up in the cytoplasm, promoting cell death[99]. In a study published in the Courtesy of Molecular Cell, Fanning *et al*. pointed out SCD, the enzyme responsible for the conversion of 18:0 into 18:1 as a potential new drug target to preserve neuronal health[99]. The team hypothesized that high levels of 18:1 promoted the binding of α-Syn to the cell membrane, increasing toxicity. Interestingly, it seemed like the relationship between α-Syn and 18:1 was a vicious circle, as high levels of α-Syn promoted the production of the FA. By inducing yeast with human α-Syn, Fanning *et al*. found that these cells overproduced 18:1, up to 60-fold excess[99]. Furthermore, the addition of exogenous 18:1 to the yeast cultures provoked cell death in the α-Syn positive cultures and not in the wild-type yeast. Cells were, however, rescued by turning off the yeast ortholog of SCD. The experiment was repeated in several cell lines, including patient cell lines and mouse models of familial PD. All cell lines gave the same result, clearing indicating oleic acid as a mediator of α-Syn toxicity. These findings suggest that age-related elevations in oleic acid may contribute to α-Syn aggregation, ultimately leading to the toxic oligomers and fibrils found in PD brains.

LC-MS/MS also found a senescence-related decrease in the 16:0/16:1 ratio, but due to the high standard deviation (64.7 ± 44.3%), no conclusion could be drawn from these results.

6.3.4 - Decrease in Arachidonic Acid Content

Another LC-MS/MS result that could have implications for PD, is the 45.8 ± 2.2% decrease in AA detected with LC-MS/MS (Figure 5.3.3b). This polyunsaturated omega-6 FA servs many important functions in the brain, including an involvement in synaptic signaling, neuronal firing, neurotransmitter release, the sleep cycle, and appetite control[100]. Many of these functions are altered in neurodegenerative diseases, suggesting a connection between brain AA metabolism and PD. Indeed, a study by P. Teismann *et al*. discovered that PD is associated with an upregulation of cyclooxygenase type 2 (COX-2), an enzyme responsible for the conversion of AA into the precursor of several prostanoids, which are mediators of inflammatory reactions [101]. The study further suggested that the neurodegenerative consequence of elevated COX-2 levels was increased oxidative damage. Assuming the same phenomenon occurs with aging, increased COX-2 activity could explain the decrease in AA found in the senescent cells. And as a consequence, altered AA metabolism could have implications for the AA-associated neuronal functions mentioned above.

6.3.5 – Presence of Short Fatty Acid Chains (10-12 carbons)

Although no major differences were observed in the overall length of the FAs between the samples, some short-chained FAs (10-12 carbons) were detected in the senescent cells and not in any of the four untreated samples (Figure 5.3.4). This result is yet another finding which could be implicated in α-Syn pathology as membrane-induced aggregation only seems to be enhanced in the presence of lipids with short FA chains[41]. Moreover, some researchers have discovered a possible connection between gut microbes and α-Syn pathology, involving short-chained FAs[102]. The researchers proposed that short-chain FAs, produced by the microbes, mediated the disease cascade by escalating neuroinflammation. Furthermore, when inoculating PD-induced mice with fecal bacteria taken from human PD patients, their symptoms worsened. These findings suggest that gut microbes may accelerate the course of the disease by secreting enough FAs to active a neuroinflammation response.

6.4 How the COVID-19 Pandemic Affected This Thesis

The sudden disruption of laboratory work, due to the outbreak of the COVID-19 virus, left several already readily prepared lipid isolates in the -20°C freezer. These samples included three A-431 samples for ^{31}P NMR, one senescence-induced SH-SY5Y sample for ^{31}P NMR, four A-431 samples for LC-MS/MS, and three treated SH-SY5Y samples for LC-MS/MS. Some of the LC-MS/MS samples were run after the lab had reopened, but no lipids were detected in any of the samples, most likely due to lipid degradation during the lab-shutdown. Another experiment affected by the time-restrictions of COVID-19 was a Western Blot (WB) to determine the upregulations of p21 and p16 in the treated cells – another confirmation of cellular senescence. Several WB was attempted but needed to be optimized to get the proper results. A toxicity assay was also attempted, but as with the WB, that would require more lab-time to be optimized.

6.3 Conclusion

Altogether, there seem to be several age-related alterations to the lipid composition of neurons that could increase a person's likelihood of developing neurodegenerative disorders like PD. These alterations include an increase in the abundance of negatively charged lipids like PS and PI (Figure 5.2.1b), a decrease in the abundance of AA (Figure 5.3.3b), changes to the 18:0/18:1 ratio (Figure 5.3.3c) and a decrease in the total amount of PUFAs with a similar decrease in MUFAs (Figure 5.3.3a). Although none of these findings alone can explain why age poses the greatest risk factor for developing PD, they do reveal the major impact aging has on the lipidome. Furthermore, the striking similarities between the normal aging process and the development of PD suggest that aging provides a cellular environment more susceptible to the neuronal toxic mechanisms associated with PD. One example of this, is the increase in the PI and PS content. Although negatively charged lipids alone do not increase the probability of α-Syn aggregation, in combination with elevated protein levels they may induce aggregation. Moreover, if PUFA (in particular AA) levels also are altered, affecting neuronal repair and health, this may further implicate the toxic consequence of the newly formed aggregates. Nevertheless, seeing as PD is not a normal part of aging, there seems to be a necessity for an additional cause, possibly mutations in genes implicated in cellular homeostasis, in order to develop the disease. As aging increase mutation rates on a general basis, the combination of mutations and age-related lipid alterations may be the key to the vast prevalence of PD among the elderly (Figure 6.3.1).

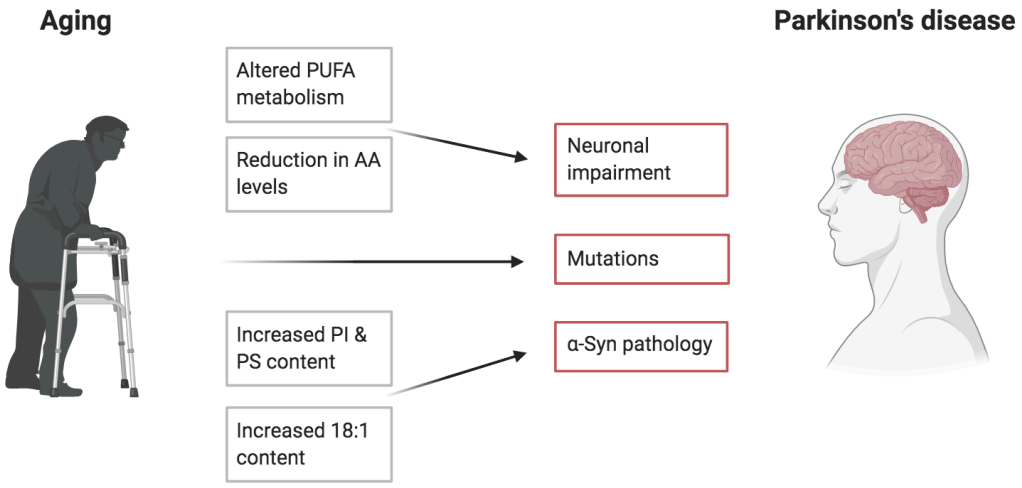

Figure 6.3.1 – Findings with implications for the development of PD. Changes detected in senescence-induced SH-SY5Y cells which could increase a person's risk of developing PD, including a reduction in the abundance of polyunsaturated fatty acids (PUFAs), reduction in arachidonic acid (AA), increase in the abundance of phosphatidylinositol (PI) and phosphatidylserine (PS).

6.4 Future perspective

Based on the results in this study, it would be interesting to gain more information about the individual findings by looking at the gene expression of enzymes involved in lipid metabolism using qPCR or RNA sequencing. More specifically, looking at enzymes involved in PI and PS metabolism, COX-2 involved in AA metabolism as well as SCD, responsible for the conversion of 18:0 into 18:1. One could also look for enzymes involved in the conversion of long FA into short-chained acids. Knowledge about all of these enzymes would help support the initial findings made in this thesis. Another interesting experiment could be a toxicity assay, comparing the viability of senescent and untreated cells after incubation with toxic α-Syn oligomers.

Also, to ensure that the results are relevant in a biomedical context, it would be smart to quality-check and optimize the SH-SY5Y cell line used in this study. Seeing as these cells originate from cancer cells an idea could be to investigate if their lipid composition corresponds to those of healthy neuronal cells, possibly by comparing the lipid profile of SH-SY5Y cells with dopaminergic neurons obtained from brain tissues of human subjects. The next step could be an optimization of the cell line, as the cell cultures used for these experiments contain a mixture of undifferentiated neurons-like and epithelial-like cells. A way to accomplish this could be the combination of serum starvation and the addition of retinoic acid, as the former has been shown to induce apoptosis in epithelial cells, whilst the latter activates tyrosine receptor B in neuronal cells, leading to cell survival[103]. By subsequently introducing the cells to extracellular matrix proteins and neurotrophic factors, the neuron-like cells start to differentiate, resulting in a homogeneous population of mature neurons[104] [105]. However, although this could be achieved in theory, in practice the combination of the two treatments (etoposide and differentiation) could be too tough for the cells.

Another limitation of this study is the use of whole-cell lipid fractions instead of membrane isolates. To get more precise data regarding changes to the membrane lipid composition, the membrane would have to be isolated and the experiments repeated on the membrane isolates. Also, more replicates would have to be made to get reliable results. That being said, the results do provide some interesting insights into the similarities of the normal aging process and the pathology of PD.

7 References

1 Sweeney, P. *et al.* Protein misfolding in neurodegenerative diseases: implications and strategies. *Transl Neurodegener* 6, 6, doi:10.1186/s40035-017-0077-5 (2017).

2 Stefani, M. Protein folding and misfolding on surfaces. *Int J Mol Sci* 9, 2515-2542, doi:10.3390/ijms9122515 (2008).

3 Lim, J. & Yue, Z. Neuronal aggregates: formation, clearance, and spreading. *Dev Cell* 32, 491-501, doi:10.1016/j.devcel.2015.02.002 (2015).

4 de Lau, L. M. L. & Breteler, M. M. B. Epidemiology of Parkinson's disease. *The Lancet Neurology* 5, 525-535, doi:10.1016/s1474-4422(06)70471-9 (2006).

5 Tysnes, O. B. & Storstein, A. Epidemiology of Parkinson's disease. *J Neural Transm (Vienna)* 124, 901-905, doi:10.1007/s00702-017-1686-y (2017).

6 Sneha Mantri, J. F. M. Prodromal and Early Parkinson's Disease Diagnosis. *Practical Neurology* (2018).

7 Boulos, C., Yaghi, N., El Hayeck, R., Heraoui, G. N. & Fakhoury-Sayegh, N. Nutritional Risk Factors, Microbiota and Parkinson's Disease: What Is the Current Evidence? *Nutrients* 11, doi:10.3390/nu11081896 (2019).

8 Goldman, S. M. *et al.* Head injury and Parkinson's disease risk in twins. *Ann Neurol* 60, 65-72, doi:10.1002/ana.20882 (2006).

9 Kamel, F. *et al.* Dietary fat intake, pesticide use, and Parkinson's disease. *Parkinsonism Relat Disord* 20, 82-87, doi:10.1016/j.parkreldis.2013.09.023 (2014).

10 Reeve, A., Simcox, E. & Turnbull, D. Ageing and Parkinson's disease: why is advancing age the biggest risk factor? *Ageing Res Rev* 14, 19-30, doi:10.1016/j.arr.2014.01.004 (2014).

11 Dorsey, E. R. *et al.* Global, regional, and national burden of Parkinson's disease, 1990–2016: a systematic analysis for the Global Burden of Disease Study 2016. *The Lancet Neurology* 17, 939-953, doi:10.1016/s1474-4422(18)30295-3 (2018).

12 Pringsheim, T., Jette, N., Frolkis, A. & Steeves, T. D. The prevalence of Parkinson's disease: a systematic review and meta-analysis. *Mov Disord* 29, 1583-1590, doi:10.1002/mds.25945 (2014).

13 Wirdefeldt, K., Adami, H. O., Cole, P., Trichopoulos, D. & Mandel, J. Epidemiology and etiology of Parkinson's disease: a review of the evidence. *Eur J Epidemiol* 26 Suppl 1, S1-58, doi:10.1007/s10654-011-9581-6 (2011).

14 Wright Willis, A., Evanoff, B. A., Lian, M., Criswell, S. R. & Racette, B. A. Geographic and ethnic variation in Parkinson disease: a population-based study of US Medicare beneficiaries. *Neuroepidemiology* 34, 143-151, doi:10.1159/000275491 (2010).

15 Sarika Srivastava, M. C. H. Role of Sirtuins and Calorie Restriction in Neuroprotection: Implications in Alzheimers's and Parkinson's Diseases. *Current Pharmaceutical Design* 17, 3418-3433, doi:10.2174/138161211798072526 (2011).

16 Van Maele-Fabry, G., Hoet, P., Vilain, F. & Lison, D. Occupational exposure to pesticides and Parkinson's disease: a systematic review and meta-analysis of cohort studies. *Environ Int* 46, 30-43, doi:10.1016/j.envint.2012.05.004 (2012).

17 Brown, T. P., Rumsby, P. C., Capleton, A. C., Rushton, L. & Levy, L. S. Pesticides and Parkinson's disease--is there a link? *Environ Health Perspect* 114, 156-164, doi:10.1289/ehp.8095 (2006).

18 Klein, C. & Westenberger, A. Genetics of Parkinson's disease. *Cold Spring Harb Perspect Med* 2, a008888, doi:10.1101/cshperspect.a008888 (2012).

19 Friederich Heinrich Lewy, E. F. *Handbuch der Neurologie*. Vol. 3 (1912).

20 Engelhardt, E. & Gomes, M. D. M. Lewy and his inclusion bodies: Discovery and rejection. *Dement Neuropsychol* 11, 198-201, doi:10.1590/1980-57642016dn11-020012 (2017).

21 Galvin, J. E., Schuck, T. M., Lee, V. M. & Trojanowski, J. Q. Differential expression and distribution of alpha-, beta-, and gamma-synuclein in the developing human substantia nigra. *Exp Neurol* 168, 347-355, doi:10.1006/exnr.2000.7615 (2001).

22 Bridi, J. C. & Hirth, F. Mechanisms of alpha-Synuclein Induced Synaptopathy in Parkinson's Disease. *Front Neurosci* 12, 80, doi:10.3389/fnins.2018.00080 (2018).

23 Qin, Z., Hu, D., Han, S., Hong, D. P. & Fink, A. L. Role of different regions of alpha-synuclein in the assembly of fibrils. *Biochemistry* 46, 13322-13330, doi:10.1021/bi7014053 (2007).

24 Bisaglia, M. *et al.* Structure and topology of the non-amyloid-beta component fragment of human alpha-synuclein bound to micelles: implications for the aggregation process. *Protein Sci* 15, 1408-1416, doi:10.1110/ps.052048706 (2006).

25 Galvagnion, C. The Role of Lipids Interacting with alpha-Synuclein in the Pathogenesis of Parkinson's Disease. *J Parkinsons Dis* 7, 433-450, doi:10.3233/JPD-171103 (2017).

26 Ingelsson, M. Alpha-Synuclein Oligomers-Neurotoxic Molecules in Parkinson's Disease and Other Lewy Body Disorders. *Front Neurosci* 10, 408, doi:10.3389/fnins.2016.00408 (2016).

27 Verma, M., Vats, A. & Taneja, V. Toxic species in amyloid disorders: Oligomers or mature fibrils. *Ann Indian Acad Neurol* 18, 138-145, doi:10.4103/0972-2327.144284 (2015).

28 Jove, M., Pradas, I., Dominguez-Gonzalez, M., Ferrer, I. & Pamplona, R. Lipids and lipoxidation in human brain aging. Mitochondrial ATP-synthase as a key lipoxidation target. *Redox Biol* 23, 101082, doi:10.1016/j.redox.2018.101082 (2019).

29 Dawson, G. Measuring brain lipids. *Biochim Biophys Acta* 1851, 1026-1039, doi:10.1016/j.bbalip.2015.02.007 (2015).

30 West, K., Martin, Troncoso. The CA1 Region of the Human Hippocampus Is a Hot Spot in Alzheimer's Disease. *Annals of the new york academy of sciences* (2006).

31 Canale, C. *et al.* Different effects of Alzheimer's peptide Abeta(1-40) oligomers and fibrils on supported lipid membranes. *Biophys Chem* 182, 23-29, doi:10.1016/j.bpc.2013.07.010 (2013).

32 John S. O'Brian, L. S. Lipid composition of the normal human brain: grey matter, white matter, and myelin. *Journal of Lipid Research* 6 (1965).

33 Naudi, A. *et al.* Lipidomics of human brain aging and Alzheimer's disease pathology. *Int Rev Neurobiol* 122, 133-189, doi:10.1016/bs.irn.2015.05.008 (2015).

34 Manuela Marinez, I. M. Fatty Acid Composition of Human Brain Phospholipids During Normal Development. *Journal of Neurochemistry* 71 (1998).

35 Fusco, G. *et al.* Direct observation of the three regions in alpha-synuclein that determine its membrane-bound behaviour. *Nat Commun* 5, 3827, doi:10.1038/ncomms4827 (2014).

36 Galvagnion, C. *et al.* Lipid vesicles trigger alpha-synuclein aggregation by stimulating primary nucleation. *Nat Chem Biol* 11, 229-234, doi:10.1038/nchembio.1750 (2015).

37 Rovere, M., Sanderson, J. B., Fonseca-Ornelas, L., Patel, D. S. & Bartels, T. Refolding of helical soluble alpha-synuclein through transient interaction with lipid interfaces. *FEBS Lett* 592, 1464-1472, doi:10.1002/1873-3468.13047 (2018).

38 Mori, A., Imai, Y. & Hattori, N. Lipids: Key Players That Modulate alpha-Synuclein Toxicity and Neurodegeneration in Parkinson's Disease. *Int J Mol Sci* 21, doi:10.3390/ijms21093301 (2020).

39 Ahn, M., Kim, S., Kang, M., Ryu, Y. & Kim, T. D. Chaperone-like activities of alpha-synuclein: alpha-synuclein assists enzyme activities of esterases. *Biochem Biophys Res Commun* 346, 1142-1149, doi:10.1016/j.bbrc.2006.05.213 (2006).

40 Hoyer, W. *et al.* Dependence of α-Synuclein Aggregate Morphology on Solution Conditions. *Journal of Molecular Biology* 322, 383-393, doi:10.1016/s0022-2836(02)00775-1 (2002).

41 Galvagnion, C. *et al.* Chemical properties of lipids strongly affect the kinetics of the membrane-induced aggregation of alpha-synuclein. *Proc Natl Acad Sci U S A* 113, 7065-7070, doi:10.1073/pnas.1601899113 (2016).

42 Viennet, T. *et al.* Structural insights from lipid-bilayer nanodiscs link alpha-Synuclein membrane-binding modes to amyloid fibril formation. *Commun Biol* 1, 44, doi:10.1038/s42003-018-0049-z (2018).

43 O'Leary, E. I., Jiang, Z., Strub, M. P. & Lee, J. C. Effects of phosphatidylcholine membrane fluidity on the conformation and aggregation of N-terminally acetylated alpha-synuclein. *J Biol Chem* 293, 11195-11205, doi:10.1074/jbc.RA118.002780 (2018).

44 Bodner, C. R., Dobson, C. M. & Bax, A. Multiple tight phospholipid-binding modes of alpha-synuclein revealed by solution NMR spectroscopy. *J Mol Biol* 390, 775-790, doi:10.1016/j.jmb.2009.05.066 (2009).

45 Chandra, S., Chen, X., Rizo, J., Jahn, R. & Sudhof, T. C. A broken alpha -helix in folded alpha -Synuclein. *J Biol Chem* 278, 15313-15318, doi:10.1074/jbc.M213128200 (2003).

46 Freche, D., Lee, C. Y., Rouach, N. & Holcman, D. Synaptic transmission in neurological disorders dissected by a quantitative approach. *Commun Integr Biol* 5, 448-452, doi:10.4161/cib.20818 (2012).

47 Borroni, M. V., Valles, A. S. & Barrantes, F. J. The lipid habitats of neurotransmitter receptors in brain. *Biochim Biophys Acta* 1858, 2662-2670, doi:10.1016/j.bbamem.2016.07.005 (2016).

48 Maynard, S., Fang, E. F., Scheibye-Knudsen, M., Croteau, D. L. & Bohr, V. A. DNA Damage, DNA Repair, Aging, and Neurodegeneration. *Cold Spring Harb Perspect Med* 5, doi:10.1101/cshperspect.a025130 (2015).

49 Amir S. Kahn, D. C. S., Thomas Wanneburg, Willian E. Sonntag. Growth horome, insulin-like growth factor-1 and the aging cardiovascular system. *Cardiovascular Research* 54, 25-35 (2002).

50 Goldsmith, T. C. Evolution of Aging Theories: Why Modern Programmed Aging Concepts Are Transforming Medical Research. *Biochemistry (Mosc)* 81, 1406-1412, doi:10.1134/S0006297916120026 (2016).

51 P. S. Timiras, V. J. C., D.B Hudson. Neuroendocrine pacemaker for growth, development and ageing. *Age and Ageing* 11, 73-88 (1982).

52 Kurt A. Jellinger, J. A. Neuropathological approaches to cerebral aging and neuroplasticity. *Dialogues in Clinical Neuroscience* 15 (2013).

53 McGeer. Neurotransmitters in Normal Aging. *Geriatrics* 1, 263-282 (1982).

54 Frade, J. M. & Ovejero-Benito, M. C. Neuronal cell cycle: the neuron itself and its circumstances. *Cell Cycle* 14, 712-720, doi:10.1080/15384101.2015.1004937 (2015).

55 Gorbunova, V., Seluanov, A., Mao, Z. & Hine, C. Changes in DNA repair during aging. *Nucleic Acids Res* 35, 7466-7474, doi:10.1093/nar/gkm756 (2007).

56 Collier, T. J., Kanaan, N. M. & Kordower, J. H. Aging and Parkinson's disease: Different sides of the same coin? *Mov Disord* 32, 983-990, doi:10.1002/mds.27037 (2017).

57 Soderberg, E., Kristensson, Dallner. Lipid Compositions of Different Regions of the Human Brain During Aging. *Journal of Neurochemistry* 54 (1990).

58 Horrocks, V., Yates. Lipid Changes in the Ageing Brain. *The Molecular Basis of Neuropathology* (1981).

59 Svennerholm, L. Membrane Lipids of Adult Human Brain: Lipid Composition of Frontal and Temporal Lobe in Subjects of Age 20 to 100 Years. *Journal of Neurochemistry* 63, doi:10.1046/j.1471-4159.1994.63051802.x (1994).

60 Spiteller, G. Lipid peroxidation in aging and age-dependent diseases. *Experimental Gerontology* 36, 1425-1457, doi:10.1016/s0531-5565(01)00131-0 (2001).

61 Robert K. McNamara, Y. L., Ronald Jandacek, Therese Rider, Patrick Tso. The Aging Human Orbitofrontal Cortex: Decreasing Polyunsaturated Fatty Acid Composition and Associated Increases in Lipogenic Gene Expression and Steroyl-CoA Desaturase Activity. *Prostaglandins Leukot Essent Fatty Acids* 78, 293-304 (2008).

62 Abbatecola, A. M. *et al.* Plasma polyunsaturated fatty acids and age-related physical performance decline. *Rejuvenation Res* 12, 25-32, doi:10.1089/rej.2008.0799 (2009).

63 Ioan, B. G. *et al.* The Chemistry Decomposition in Human Corpses. *Revista de Chimie* 68, 1352-1356, doi:10.37358/rc.17.6.5672 (2017).

64 Forbes, S. L. Decomposition Chemistry in a Burial Environment. *Soil Analysis in Forensic Taphonomy*, 203-223 (2008).

65 van Deursen, J. M. The role of senescent cells in ageing. *Nature* 509, 439-446, doi:10.1038/nature13193 (2014).

66 Hayflick, M. The serial cultication of human diloid cell strains. *Experimental Cell Research* 25, 585-621 (1961).

67 Hernandez-Segura, A., Nehme, J. & Demaria, M. Hallmarks of Cellular Senescence. *Trends Cell Biol* 28, 436-453, doi:10.1016/j.tcb.2018.02.001 (2018).

68 D. E. Comings, T. A. O. Electron Microscopy of Human Fibroblast in Tissue Culture during Logatithmic and Confluent Stages of Growth. *Experimental Cell Research* 61, 295-301, doi:10.1016/0014-4827(70)90451-9 (1970).

69 David J. Kurz, S. D., Ying Hong, Jorge D. Erusalimsky. Senescence-assosiated beta-galactosidase reflects an increase in lysosomal mass during replicative ageing of human endothelial cells. *Journal of Cell Science* 113, 3613-3622 (200).

70 GOberdhan P. Dimri, X. L., George Basile. A biomarker that identifies senescent human cells in culture and in aging skin invivo. *Cell Biology* 92, 9363-9367 (1995).

71 Edward M. Brown, Z. C., Nicoletta Crescenzio, Katharina D'Herde. *Cell Apoptosis Research Advances*. (2007).

72 Lye, J. J. *et al.* Astrocyte senescence may drive alterations in GFAPalpha, CDKN2A p14(ARF), and TAU3 transcript expression and contribute to cognitive decline. *Geroscience* 41, 561-573, doi:10.1007/s11357-019-00100-3 (2019).

73 Sofroniew, M. V. & Vinters, H. V. Astrocytes: biology and pathology. *Acta Neuropathol* 119, 7-35, doi:10.1007/s00401-009-0619-8 (2010).

74 Yan Li1, Forough Ghasemi Naghdi1, Sourabh Garg1, Tania Catalina Adarme-Vega1, Kristofer J Thurecht3, Wael Abdul Ghafor3, Simon Tannock1, Peer M Schenk1. A comparative study: the impact of different lipid extraction methods on current microalgal lipid research. *Microbial Cell factories* 13 (2014).

75 Dyer, E. G. B. W. J. A Rapid Method of Total Lipid Extraction and Purification. *Canadian Journal of Biochemistry and Physiology* 37, doi: (1959).

76 Folch, J. A Simple Method for the Isolation and Purification of Total Lipides from Animal Tissues. *The Journal of Biological Chemistry* 226, 497-509 (1956).

77 Emwas, A. H. The strengths and weaknesses of NMR spectroscopy and mass spectrometry with particular focus on metabolomics research. *Methods Mol Biol* 1277, 161-193, doi:10.1007/978-1-4939-2377-9_13 (2015).

78 Khoury, S. *et al.* Quantification of Lipids: Model, Reality, and Compromise. *Biomolecules* 8, doi:10.3390/biom8040174 (2018).

79 Kushnir, M. M., Rockwood, A. L. & Bergquist, J. Liquid chromatography-tandem mass spectrometry applications in endocrinology. *Mass Spectrom Rev* 29, 480-502, doi:10.1002/mas.20264 (2010).

80 Kang, J.-S. Principles and Applications of LC-MS/MS for the Quantitative Bioanalysis of Analytes in Various Biological Samples. *InTech* (2012).

81 Koelmel, J. P. *et al.* Expanding Lipidome Coverage Using LC-MS/MS Data-Dependent Acquisition with Automated Exclusion List Generation. *J Am Soc Mass Spectrom* 28, 908-917, doi:10.1007/s13361-017-1608-0 (2017).

82 Xicoy, H., Wieringa, B. & Martens, G. J. The SH-SY5Y cell line in Parkinson's disease research: a systematic review. *Mol Neurodegener* 12, 10, doi:10.1186/s13024-017-0149-0 (2017).

83 Shipley, M. M., Mangold, C. A., Kuny, C. V. & Szpara, M. L. Differentiated Human SH-SY5Y Cells Provide a Reductionist Model of Herpes Simplex Virus 1 Neurotropism. *J Virol* 91, doi:10.1128/JVI.00958-17 (2017).

84 Cremonini, M. A., Laghi, L. & Placucci, G. Investigation of commercial lecithin by31P NMR in a ternary CUBO solvent. *Journal of the Science of Food and Agriculture* 84, 786-790, doi:10.1002/jsfa.1683 (2004).

85 Bosco, M., Culeddu, N., Toffanin, R. & Pollesello, P. Organic solvent systems for 31P nuclear magnetic resonance analysis of lecithin phospholipids: applications to two-dimensional gradient-enhanced 1H-detected heteronuclear multiple quantum coherence experiments. *Anal Biochem* 245, 38-47, doi:10.1006/abio.1996.9907 (1997).

86 Emwas, A. H. *et al.* Recommended strategies for spectral processing and post-processing of 1D (1)H-NMR data of biofluids with a particular focus on urine. *Metabolomics* 14, 31, doi:10.1007/s11306-018-1321-4 (2018).

87 Furse, S. *et al.* The lipidome and proteome of oil bodies from Helianthus annuus (common sunflower). *J Chem Biol* 6, 63-76, doi:10.1007/s12154-012-0090-1 (2013).

88 Jakubec, M., Barias, E., Kryuchkov, F., Hjornevik, L. V. & Halskau, O. Fast and Quantitative Phospholipidomic Analysis of SH-SY5Y Neuroblastoma Cell Cultures Using Liquid Chromatography-Tandem Mass Spectrometry and (31)P Nuclear Magnetic Resonance. *ACS Omega* 4, 21596-21603, doi:10.1021/acsomega.9b03463 (2019).

89 Murgia, S. Quantitative Characterization of Phospholipids in Milk Fat via 31P NMR Using a Monophasic Solvent Mixture. *Lipids* 38 (2003).

90 <J. Lipid Res.-1986-Sotirhos-386-92.pdf>.

91 Casares, D., Escriba, P. V. & Rossello, C. A. Membrane Lipid Composition: Effect on Membrane and Organelle Structure, Function and Compartmentalization and Therapeutic Avenues. *Int J Mol Sci* 20, doi:10.3390/ijms20092167 (2019).

92 LoPiccolo, J., Blumenthal, G. M., Bernstein, W. B. & Dennis, P. A. Targeting the PI3K/Akt/mTOR pathway: effective combinations and clinical considerations. *Drug Resist Updat* 11, 32-50, doi:10.1016/j.drup.2007.11.003 (2008).

93 L.A. Horrocks, G. Y. S., Robert A. DAmato. Changes in Brain Lipids During Aging. *Neurobiology of Aging*, 359-367 (1975).

94 Paradies, G., Paradies, V., De Benedictis, V., Ruggiero, F. M. & Petrosillo, G. Functional role of cardiolipin in mitochondrial bioenergetics. *Biochim Biophys Acta* 1837, 408-417, doi:10.1016/j.bbabio.2013.10.006 (2014).

95 Stillwell, W. *An Introdution to Biological Membranes*. 2 edn, (2016).

96 Zong, W. X., Rabinowitz, J. D. & White, E. Mitochondria and Cancer. *Mol Cell* 61, 667-676, doi:10.1016/j.molcel.2016.02.011 (2016).

97 Bazinet, R. P. & Laye, S. Polyunsaturated fatty acids and their metabolites in brain function and disease. *Nat Rev Neurosci* 15, 771-785, doi:10.1038/nrn3820 (2014).

98 Pao-Yen Lin, C.-C. C., Shih-Yi Huang, Kuan-Pin Su. A Meta-Analytical Review of Polyunsaturated Fatty Acid Compositions in Dementia. *The Journal of Clinical Psychiatry* 73 (2012).

99 Fanning, S. *et al.* Lipidomic Analysis of alpha-Synuclein Neurotoxicity Identifies Stearoyl CoA Desaturase as a Target for Parkinson Treatment. *Mol Cell* 73, 1001-1014 e1008, doi:10.1016/j.molcel.2018.11.028 (2019).

100 Bosetti, F. Arachidonic Acid Metabolism in Brain Physiology and Pathology: Lessons from Genetically Altered Mouse Models. *Journal of Neurochemistry* 102, 577-586 (2007).

101 Teismann, P. *et al.* Cyclooxygenase-2 is instrumental in Parkinson's disease neurodegeneration. *Proc Natl Acad Sci U S A* 100, 5473-5478, doi:10.1073/pnas.0837397100 (2003).

102 Sampson, T. R. *et al.* Gut Microbiota Regulate Motor Deficits and Neuroinflammation in a Model of Parkinson's Disease. *Cell* 167, 1469-1480 e1412, doi:10.1016/j.cell.2016.11.018 (2016).

103 Schamberger, C. J., Gerner, C. & Cerni, C. Caspase-9 plays a marginal role in serum starvation-induced apoptosis. *Exp Cell Res* 302, 115-128, doi:10.1016/j.yexcr.2004.08.026 (2005).

104 Mario Encinas, M. I., Yuhuic Liu. Sequential Treatment of SH-SY5Y Cells with Retinoic Acid and Brain-Derived Neurotrophic Factor Gives Rise to Fully Differentitated, Neurotrophic Factor-Dependent, Human Neuron-Like Cells. *Journal of Neurochemistry* 75 (2000).

105 Shipley, M. M., Mangold, C. A. & Szpara, M. L. Differentiation of the SH-SY5Y Human Neuroblastoma Cell Line. *J Vis Exp*, 53193, doi:10.3791/53193 (2016).

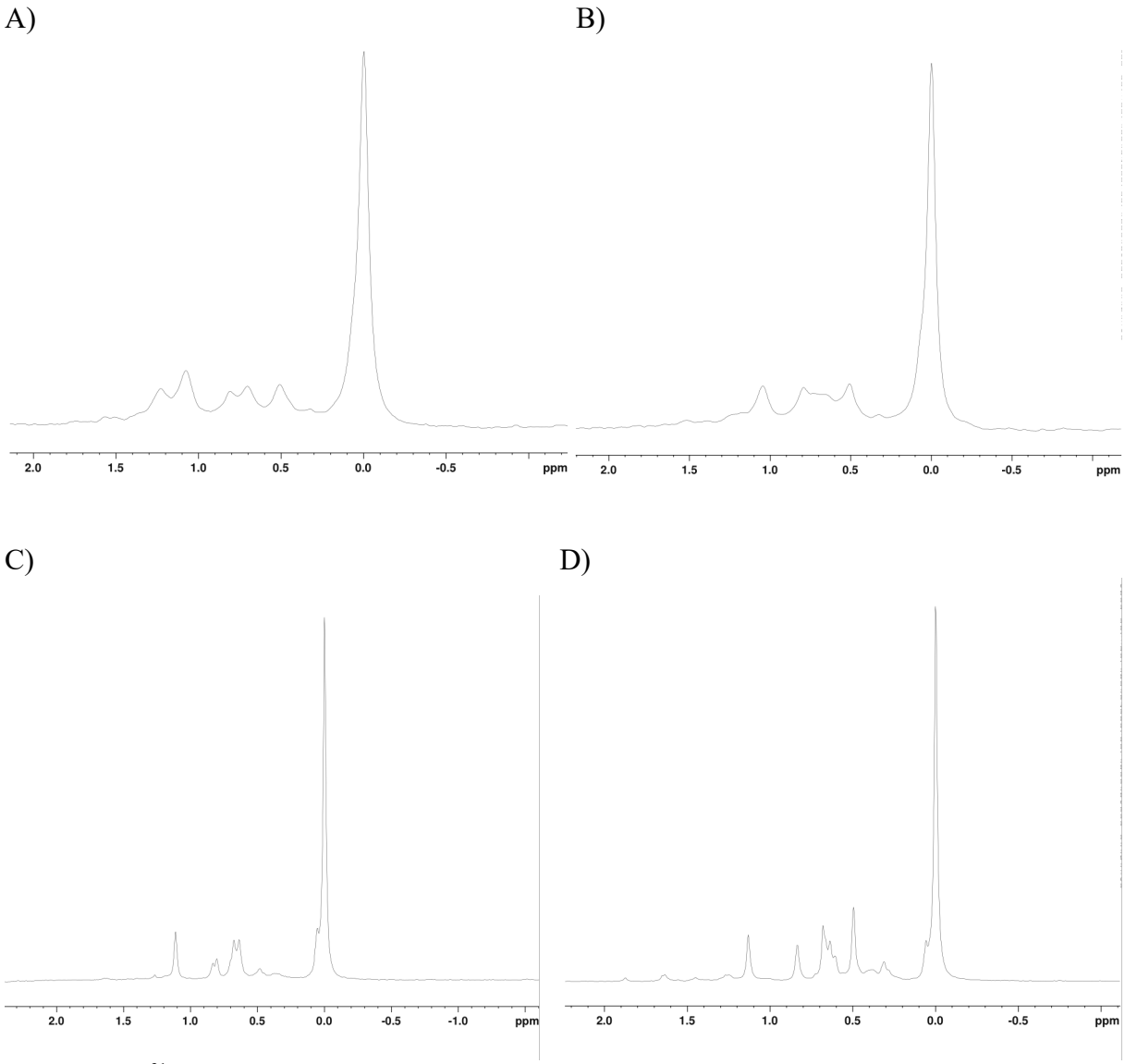

Figure 8.1 - ^{31}P NMR spectra of untreated SH-SY5Y cells. Spectra of four biological experiments are presented in A, B, C and D.

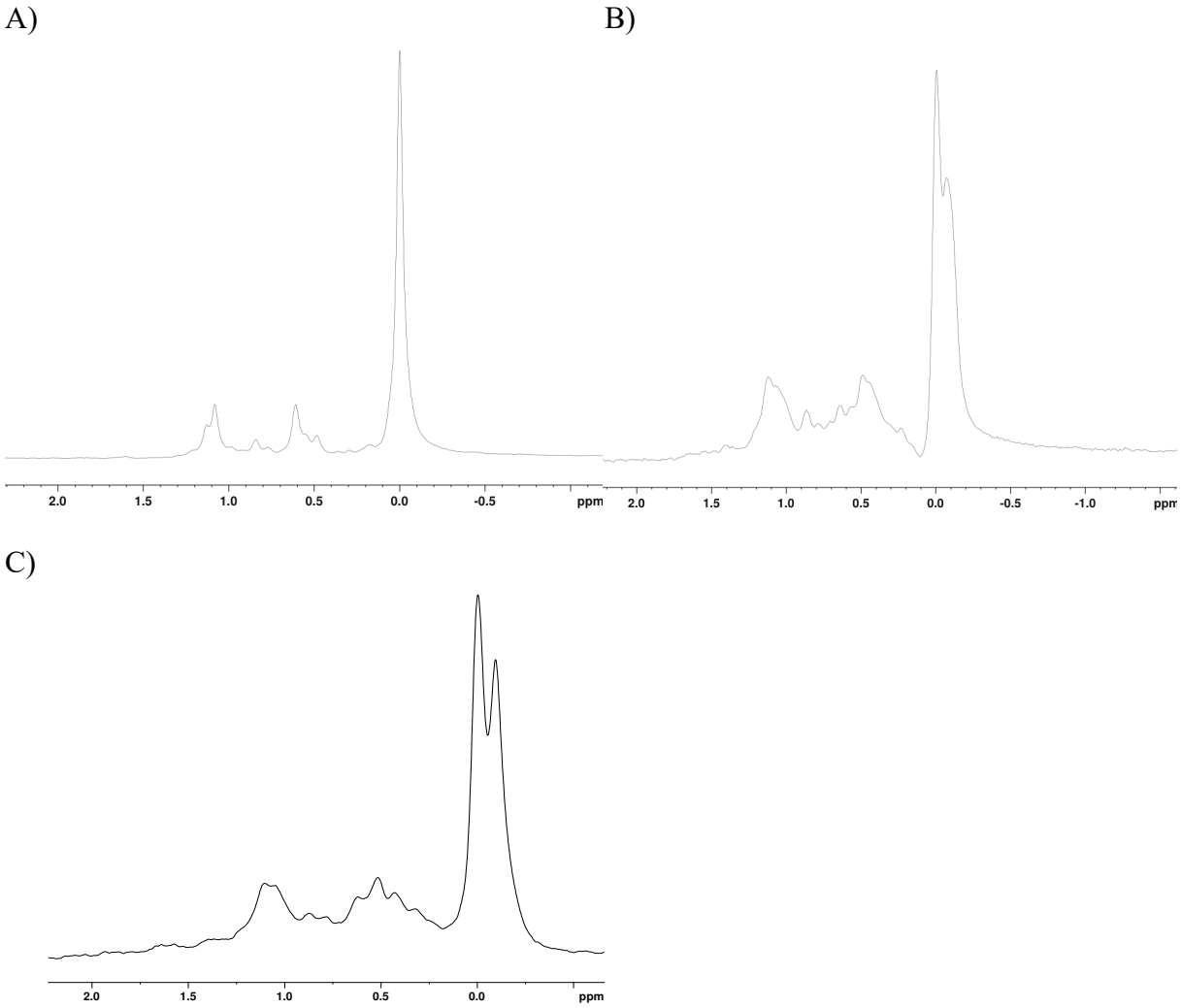

Figure 8.2 - ^{31}P NMR spectra of senescence-induced SH-SY5Y cells. Spectra of three biological experiments are presented in A, B and C.